Journal of Medicinal Chemistry

Article

pubs.acs.org/jmc

# Novel C,N-Cyclometalated Benzimidazole Ruthenium(II) and Iridium(III) Complexes as Antitumor and Antiangiogenic Agents: A Structure–Activity Relationship Study

Jyoti Yellol,[†] Sergio A. Pérez,[†] Alicia Buceta,[†] Gorakh Yellol,[†] Antonio Donaire,[†] Piotr Szumlas,[‡] Patrick J. Bednarski,[‡] Gamall Makhloufi,[§] Christoph Janiak,[§] Arturo Espinosa,[∥] and José Ruiz*[,†]

[†]Departamento de Química Inorgánica and Regional Campus of International Excellence "Campus Mare Nostrum", Universidad de Murcia and Institute for Bio-Health Research of Murcia IMIB-Arrixaca, E-30071 Murcia, Spain

[‡]Pharmaceutical and Medicinal Chemistry, Institut für Pharmazie, EMA-University of Greifswald, D-17487 Greifswald, Germany

[§]Institut für Anorganische Chemie und Strukturchemie, Heinrich-Heine-Universität Düsseldorf, Universitätsstrasse 1, D-40225 Düsseldorf, Germany

[∥]Departamento de Química Orgánica, Universidad de Murcia, E-30071 Murcia, Spain

Supporting Information

**ABSTRACT:** A series of novel C,N-cyclometalated benzimidazole ruthenium(II) and iridium(III) complexes of the types [($\eta^6$-*p*-cymene)-RuCl($\kappa^2$-*N*,*C*-L)] and [($\eta^5$-$C_5Me_5$)IrCl($\kappa^2$-*N*,*C*-L)] (HL = methyl 1-butyl-2-arylbenzimidazolecarboxylate) with varying substituents (H, Me, F, $CF_3$, MeO, $NO_2$, and Ph) in the $R_4$ position of the phenyl ring of 2-phenylbenzimidazole chelating ligand of the ruthenium (**3a**–**g**) and iridium complexes (**4a**–**g**) have been prepared. The cytotoxic activity of the new ruthenium(II) and iridium(III) compounds has been evaluated in a panel of cell lines (A2780, A2780cisR, A427, 5637, LCLC, SISO, and HT29) in order to investigate structure–activity relationships. Phenyl substitution at the $R_4$ position shows increased potency in both Ru and Ir complexes (**3g** and **4g**, respectively) as compared to their parent compounds (**3a** and **4a**) in all cell lines. In general, ruthenium complexes are more active than the corresponding iridium complexes. The new ruthenium and iridium compounds increased caspase-3 activity in A2780 cells, as shown for **3a**,**d** and **4a**,**d**. Compound **4g** is able to increase the production of ROS in A2780 cells. Furthermore, all the new compounds are able to overcome the cisplatin resistance in A2780cisR cells. In addition, some of the metal complexes effectively inhibit angiogenesis in the human umbilical vein endothelial cell line EA.hy926 at 0.5 $\mu$M, the ruthenium derivatives **3g** (Ph) and **3d** ($CF_3$) being the best performers. QC calculations performed on some ruthenium model complexes showed only moderate or slight electron depletion at the phenyl ring of the C,N-cyclometalated ligand and the chlorine atom on increasing the electron withdrawing effect of the R substituent.

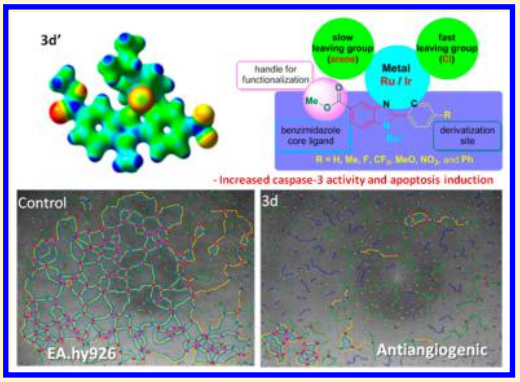


## 1. INTRODUCTION

The discovery of the anticancer activity of cisplatin by Rosenberg et al.[1] not only transformed cancer chemotherapy and broadened the range of routinely applied chemotherapeutics from organic drugs to metal-based compounds[2] but also stimulated the use of other metals in chemotherapeutics.[3] Since then, the potential of different metal-based anticancer agents has been widely explored and especially Ru, Ir, and Os complexes have been widely studied in drug discovery.[3−13] In the course of metal based anticancer drug development programs, organometallic and especially half-sandwich metal complexes have increasing demonstrated their potential.[13−35] Their hydrophobic arene ligand is thought to facilitate the diffusion through the cell membrane, while the remaining coordinating sites can be varied with different ligands to modulate biological and pharmacological properties.[17,34] In addition, angiogenesis is a hallmark of tumor development and metastasis and thus a possible target.[36,37] Furthermore, the limited survival benefits of antiangiogenic drugs have stimulated the interest in the combination of antiangiogenic drugs with established chemotherapies.[38,39] Since the ruthenium compound NAMI-A demonstrated antimetastatic activity in vivo,[40] more nontoxic ruthenium(II)[41−43] and iridium(III)[44] complexes have also been probed as angiogenesis inhibitors.

On the other hand, while recent development of Pt and Ru anticancer compounds was carried out, it was envisaged that structural modifications in ligands around the metal center can modulate the anticancer activity of the complex.[45,46] Concomitantly, Sadler et al. established a relationship between the

Received: April 26, 2015
Published: August 27, 2015





DOI: 10.1021/acs.jmedchem.5b01194
J. Med. Chem. 2015, 58, 7310−7327

hydrolysis rate for Ru(II) arene compounds and anticancer activity.[47] Ru(II) complexes containing benzimidazole (a widely used pharmacophore[48,49]) exhibited outstanding potency in anticancer,[46,50,51] antiangiogenic,[52] anti-Alzheimer,[53] and anion-sensing and photophysical[54,55] studies. In addition, an ester functionality was installed as a handle for intended functionalization of metallodrugs. Likewise, our rationally designed neutral benzimidazole C,N-cyclometalated ruthenium(II) and iridium(III) complexes exhibited good anticancer activity against HT29, T47D, A2780, and A2780cisR cancer cell lines,[46] compared to that of other relevant "piano-stool" ruthenium(II) analogues recently published.[29,56] An increasing interest for new half-sandwich iridium C,N-cyclometalated anticancer agents has been recently shown.[30]

Thus, it was supposed that the electronic effect on the metal coordinated ligand might influence the strength of metal−carbon or metal−nitrogen bond as well as the rate of metal hydrolysis which, in the end, affects the anticancer activity of the complex. With this hypothesis, we have designed the 2-phenylbenzimidazole complexes where the phenyl ring is substituted in the para position to study structure−activity relationship (SAR) of benzimidazole analogs of ruthenium and iridium complexes. The influence of electron-donating or electron-withdrawing groups, aromatic and neutral substituents on 4-position of phenyl ring of 2-arylbenzimidazole ruthenium/iridium complexes has been studied (Figure 1). SAR with

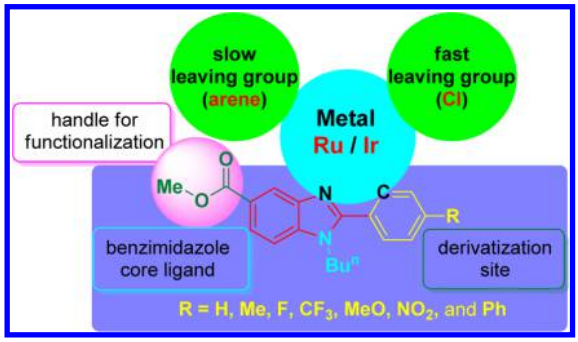


**Figure 1.** Design of the 2-phenylbenzimidazole ligand for preparation of metallodrugs.

respect to cytotoxicity, apoptosis, and cell cycle arrest in a panel of human cancer cells and antiangiogenesis studies in the endothelial cell line EA.hy926 have been investigated.

## 2. RESULTS AND DISCUSSION

**2.1. Synthesis and Characterization of the Cyclometalated Compounds.** *2.1.1. Molecular Design and Synthesis of the Modified 2-Arylbenzimidazole Ligands.* The key intermediate **1** was efficiently obtained from 4-chloro-3-nitrobenzoic acid by using reported procedures[46,53] with a few modifications (Scheme 1). Acid catalyzed methyl esterification, nucleophilic aromatic substitution of the chloro group by butylamine followed by reduction of the nitro group with zinc and ammonium formate afford **1** in an overall 60% yield. The final ligands were synthesized by condensation of intermediate **1** with appropriately substituted benzaldehyde in ethanol with catalytic amount of trifluoroacetic acid at room temperature for 16−24 h (Scheme 1). Methyl substitution was preferred initially to understand the electronically neutral but space filling substituent effect. Comparatively, a methoxy group as a strong electron donating agent and a nitro group as a

**Scheme 1. Synthesis of Main Ligands for SAR**

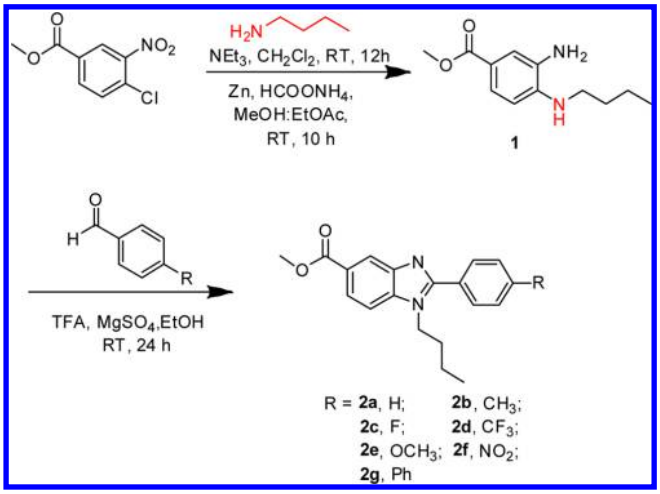


strong electron withdrawing group were considered to determine related effect on activity through physiological effect. On the other hand, fluoro and trifluoromethyl groups were also chosen for SAR studies, as fluorine can be considered "the medicinal chemist's magic element". In fact, fluorine is the most electronegative of the elements but is also relatively small in size, which means that replacing, for example, a hydrogen atom with a fluorine atom can have in general profound electronic effects on a molecule without greatly changing its overall size.[37,57,58] In addition, fluorine increases lipid solubility (bioavailability) and the strength of C−F bonds is resistant to metabolic processes.

All the ligands with different substitutions were synthesized with the same condensation method with a 50−76% yield.

*2.1.2. Synthesis of the New Cyclometalated Complexes.* Stimulated by the initial results derived from the introduction of negatively charged C,N-chelated benzimidazole ligands,[46] the synthesis of new cyclometalated benzimidazole ruthenium(II) and iridium(III) complexes was considered for SAR studies. All the ruthenium complexes were synthesized using the generalized procedure shown in Scheme 2. The benzimidazole ligand **2a−g** was treated with *p*-cymeneruthenium(II) $[(p\text{-cymene})RuCl_2]_2$ and sodium acetate in dichloromethane at room temperature for 24 h to obtain the corresponding ruthenium metal complex (**3a−g**) in moderate to good yield. The structures of the new ruthenium complexes were confirmed by spectroscopic methods. In the $^1$H NMR spectra of **3a−g** the disappearance of one aromatic proton of the 2-arylbenzimidazole ligand is observed (Supporting Information, Figure S1 for **3d**). In addition, resonances of the $\eta^6$-*p*-cymene protons were resolved to distinct peaks due to desymmetrization of the arene ligand upon complexation of the anionic chelating benzimidazole ligand at the Ru center. The positive-ion ESI-MS spectra displayed the $[M + 1]^+$ peaks with the expected isotopic distribution pattern (Supporting Information, Figure S2 for **3d**). Similarly, the half-sandwich iridium(III) complexes (**4a−g**) were prepared using a similar method starting from the corresponding pentamethylcyclopentadienyl-chloridoiridium(III) in good yields. The structures were also established by spectroscopic and analytical methods, including COSY, HSQC NMR, and ESI-MS techniques (Supporting Information, Figures S3−S7 for **4d**). The new compounds are soluble in solvents such as $CDCl_3$, DMSO, or DMF.



DOI: 10.1021/acs.jmedchem.5b01194
J. Med. Chem. 2015, 58, 7310−7327

**Scheme 2. Synthesis of Metal Complexes**

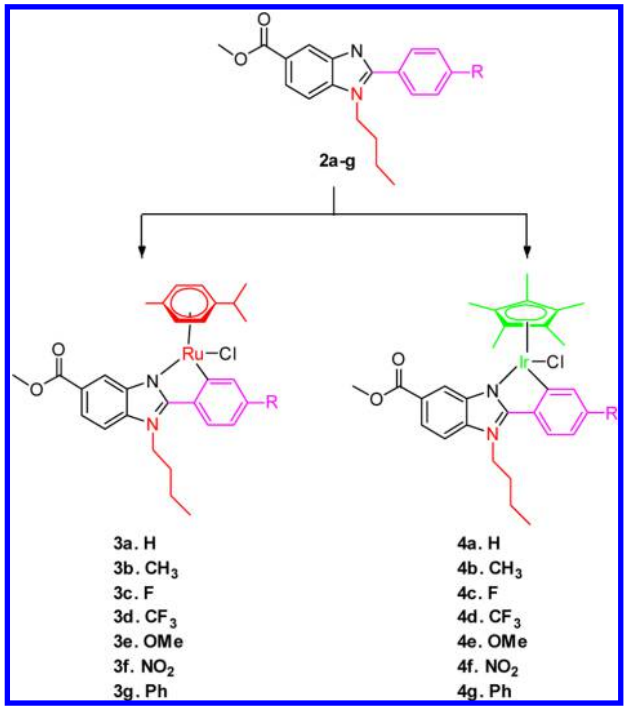


*2.1.3. Structures Determination.* Single crystals suitable for X-ray diffraction analysis were obtained from the slow diffusion of hexane into a saturated solution of **3d** and **4d** in $CH_2Cl_2$/toluene. Their structures and atom numbering schemes are shown in Figure 2. Crystallographic data are shown in Tables S1 and S4 in the Supporting Information, and selected bond lengths and angles are listed in Tables S2 and S5 in the Supporting Information. The unit cell of **3d** shows the two possible enantiomers ($R_{Ru}$ and $S_{Ru}$) resulting from the stereogenic nature of the metal center. As shown in Figure 2a, complex **3d** adopts the classical pseudooctahedral three-legged piano-stool arrangement, and hence, the arene ring displays the common $\pi$-bonded $\eta^6$-coordination mode, whereas the arylbenzimidazole-type ligand assumes a bidentate chelate coordination mode ($\kappa^2$-C,N), occupying two coordination positions. Both Ru–$cym_{centroid}$ distance for **3d** [1.712(1) Å] and Ru–Cl bond distance [2.4191(4) Å] are standard compared to alike complexes.[51] The orthometalated Ru–C distance [Ru–C = 2.0508(18) Å] is shorter than Ru–N [Ru–N = 2.0666(14) Å] but similar to the Ru–C distances of related complexes. These features result from the strong $\sigma$-donor nature of the negatively charged C atom.[59] The packing in the structure of **3d** is organized by intermolecular C–H···F,[60] C–H···Cl,[61] C–H···O,[62] and C–H···$\pi$ interactions[63] (Supporting Information, Table S3 and Figure S8). There are no $\pi$–$\pi$ interactions.[64]

Figure 2b depicts the ORTEP diagram of complex **4d**, confirming its "piano-stool" structure with the pentamethylcyclopentadienyl group displaying the common $\pi$-bonded $\eta^5$ coordination mode, whereas the 1-butyl-2-phenylbenzimidazole carboxylate assumes a bidentate-chelate coordination mode ($\kappa^2$-*C,N*), the two rings of the benzimidazole and phenyl moieties not being strictly coplanar. The orthometalated Ir–C distance [2.059(14)] is similar to that of Ir–N 2.060(11) Å. The Ir–centroid distance for **4d** is 1.81(2) Å. The Ir–Cl bond distance [2.406(3) Å] is similar to that previously[46] observed [2.4050(11) Å] for **4a**.

*2.1.4. Electrostatic Potential Surface.* With the aim of exploring the little influence observed in activities upon peripheral substitution at the C,N-cyclometalated ligand, QC calculations were performed on ruthenium model complexes **3′a**,**b**,**d** featuring a methyl (instead of butyl) group at N, as well as an electron donating (**3′b**, R = $CH_3$) or withdrawing group (**3′d**, R = $CF_3$) or none (**3′a**, R = H) at the derivatization site. Electrostatic potential (ESP) isocontour plots at the plane orthogonal to the Ru–Cl bond and containing the ruthenium atom (Figure 3a–c) show little differences in the proximity of the metal atom among the three substitution patterns, in agreement with the roughly same natural charge at Ru ($q^N$ = 0.275, 0.275, and 0.273 *e*, for **3′b**, **3′a**, and **3′d**, respectively). Also, mapping of ESP at a electron density isosurface (0.04 au) for the same three model complexes (Figure 3d–f) shows systematic higher electron density at the formally C-anionic phenyl ligand in comparison to the N-donor benzoimidazole ring system. Main observable differences along the series **3′b**/**3′a**/**3′d** consist of moderate or slight electron depletion at the

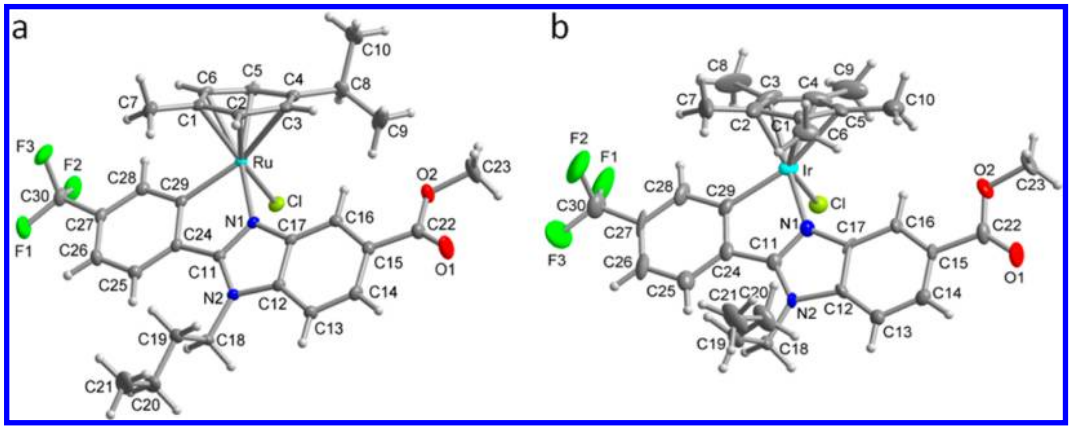


**Figure 2.** Molecular structures with atom numbering schemes for (a) **3d** (50% thermal ellipsoids) and (b) **4d** (50% thermal ellipsoids). Selected bond lengths (Å) and angles (deg) for **3d**: Ru–C29 = 2.0508(18), Ru–N1 = 2.0666(14), Ru–Cl = 2.4191(4), Ru–cym(centroid) = 1.712(1), C29–Ru–N1 = 76.64(6), N1–Ru–Cl = 86.77(4), C29–Ru–Cl = 87.68(5), cym(centroid)–Ru–Cl = 128.26(6), cym(centroid)–Ru–N1 = 131.30(7), cym(centroid)–Ru–C29 = 129.02(7). Selected bond lengths (Å) and angles (deg) for **4d**: Ir–C29 = 2.059(14), Ir–N1 = 2.060(11), Ir–Cl = 2.406(3), Ir–Cp*(centroid) = 1.81(2), C29–Ir–N1 = 76.8(5), N1–Ir–Cl = 85.6(3), C29–Ir–Cl = 88.7(4), Cp*(centroid)–Ir–Cl = 125.6(7), Cp*(centroid)–Ir–N1 = 133.1(7), Cp*(centroid)–Ir–C29 = 130.4(7).



DOI: 10.1021/acs.jmedchem.5b01194
J. Med. Chem. 2015, 58, 7310–7327

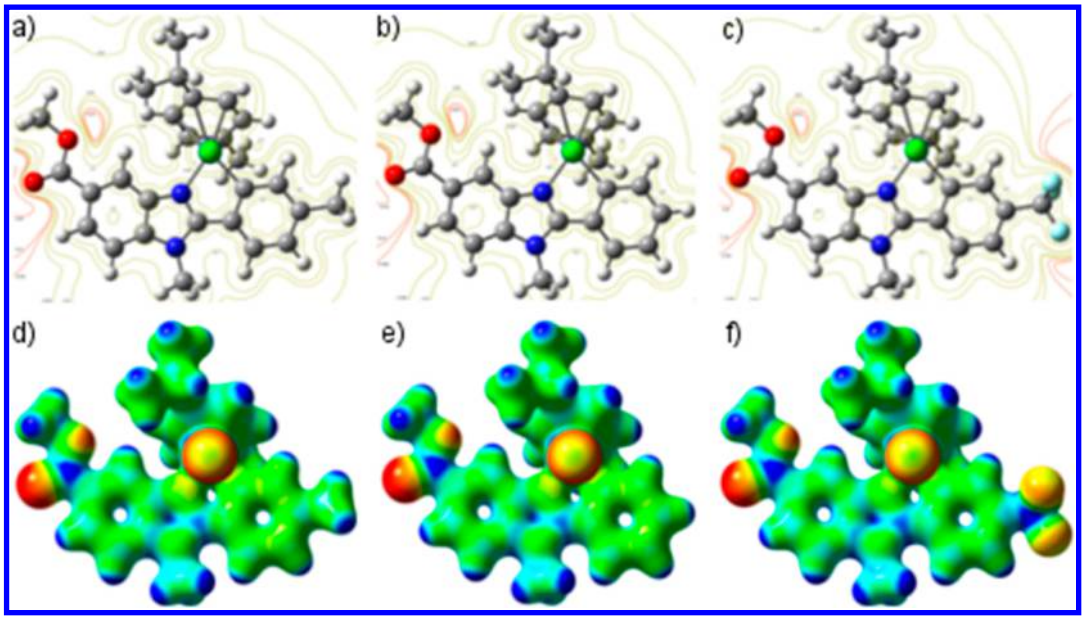


**Figure 3.** Computed (B3LYP-D3/def2TZVPPecp) ESP contour plots (0.005, 0.01, 0.05, 0.1, 0.5, and 1 au isovalues) at the plane containing the metal and orthogonal to the Ru−Cl bond, for (a) **3′b**, (b) **3′a**, and (c) **3′d**. Second row (d−f): ESP maps (from −0.02 au in red, to +0.25 au in blue) drawn onto an electron density isosurface (0.04 au) for the same compounds.

phenyl ring and the chlorine atom on increasing the electron withdrawing effect of the R substituent, which parallels the decrease of negative charge at Cl ($q^N$ = −0.495, −0.494, and −0.489 *e*, for **3′b**, **3′a** and **3′d**, respectively) therefore resulting in a slightly less-polarized stronger Ru−Cl bond (WBI= 0.521, 0.521 and 0.525, $\rho(r)$ = 0.0740, 0.0742, and 0.0746 au, for **3′b**, **3′a** and **3′d**, respectively). The *p*-cymene ligand buffers most of the electron effect of the substituent, as observed by the larger charge differences along the (*p*-cymene)RuCl moiety: $q^N$ = 0.015, 0.017, and 0.041 *e*, for **3′b**, **3′a**, and **3′d**, respectively.

*2.1.5. Hydrolysis Studies.* The easy hydrolysis of some metal half-sandwich complexes has been previously reported.[35,65] Methanol was required to ensure the solubility of the complexes in aqueous solution. The $^1$H NMR spectra of complex **3b** (∼0.5 mM) in MeOD-$d_4$ and in 25% MeOD-$d_4$/75% $D_2O$ (v/v) at 37 °C are shown in Figure 4A and Figure 4B, respectively, indicating that hydrolysis took place even in the presence of adventitious water. On the other hand, the ESI-MS results of **3b** in 25% v/v methanol/water (in the presence of ammonium formiate) show a set of peaks centered at *m*/*z* 557.17 showing the Ru isotope pattern, which is compatible with the formation of the aqua ruthenium(II) complex ([M − $H_2O$]$^+$). In order to check the reversibility of the hydrolysis, NaCl (0.5 mM and 1 mM) was added to two different samples of solution of **3b** in MeOD-$d_4$/$D_2O$; however, the same pattern of signals as in Figure 4B was again observed (Figure 4C and Figure 4D, respectively), and abundant precipitation of the complexes was observed. Similar behavior was found when **3b** and **3g** were dissolved in 25% MeOD-$d_4$/75% $D_2O$ (v/v). No iridium complexes were studied by NMR because of their low solubility.

*2.1.6. Relative Hydrophobicity.* The RP-UPLC of complexes **3b**,**c**,**g** (∼10 μM) dissolved in 10% v/v methanol in water (to ensure solubility of the complexes) has been undertaken in order to determine the relative hydrophobicities (the mobile phases used were A = $H_2O$ with 0.2% HCOOH and B = acetonitrile). The more hydrophobic complexes should have longer retention times ($t_R$).[65] As expected the order of

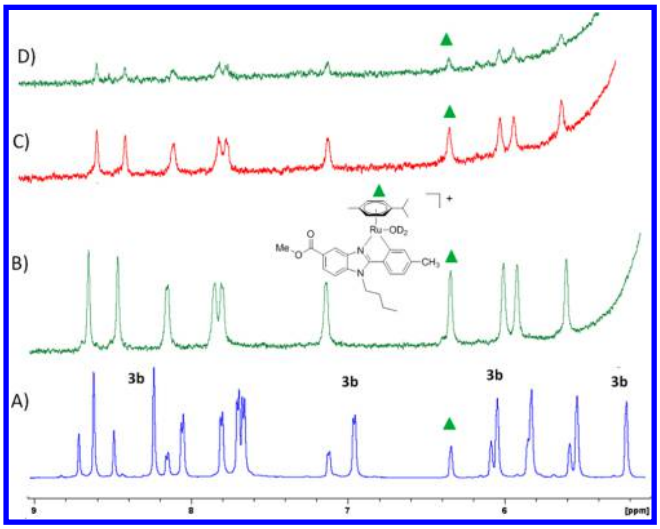


**Figure 4.** $^1$H NMR (600 MHz) spectra of complex **3b** (∼0.5 mM) in (A) MeOD-$d_4$ (containing adventitious water) and (B) 25% MeOD-$d_4$/75% $D_2O$ (v/v) after 10 min at 37 °C. Addition of NaCl 0.5 mM (C) and NaCl 1 mM (D), respectively, to two different samples of (B).

retention time follows (Figure 5) the sequence **3c** < **3b** < **3g**. The QTOF-MS of the ∼5.9 min of **3g** shows the ruthenium isotopic pattern at *m*/*z* 561.15, which could be assigned to [**3g** − Cl]$^+$ or to the loss of $H_2O$ from the corresponding aqua-ruthenium complex (see section 2.1.5). A similar behavior was observed for **3b** and **3c**.

**2.2. Biological Activity.** *2.2.1. Cytotoxicity Studies.* The cytotoxicity of the new complexes **3a−g** and **4a−g** was evaluated toward a panel of human cancer cell lines, including A2780 (human ovarian cancer cells), A2780cisR (acquired resistance to cisplatin, CDDP), 5637 (human bladder cancer cells), A427, LCLC-103H (both human lung carcinoma cells), SISO (human uterine cervical adenocarcinoma cells), and HT29 (human colorectal adenocarcinoma cells). Because of the low aqueous solubility of the complexes, the tested compounds


DOI: 10.1021/acs.jmedchem.5b01194
J. Med. Chem. 2015, 58, 7310−7327

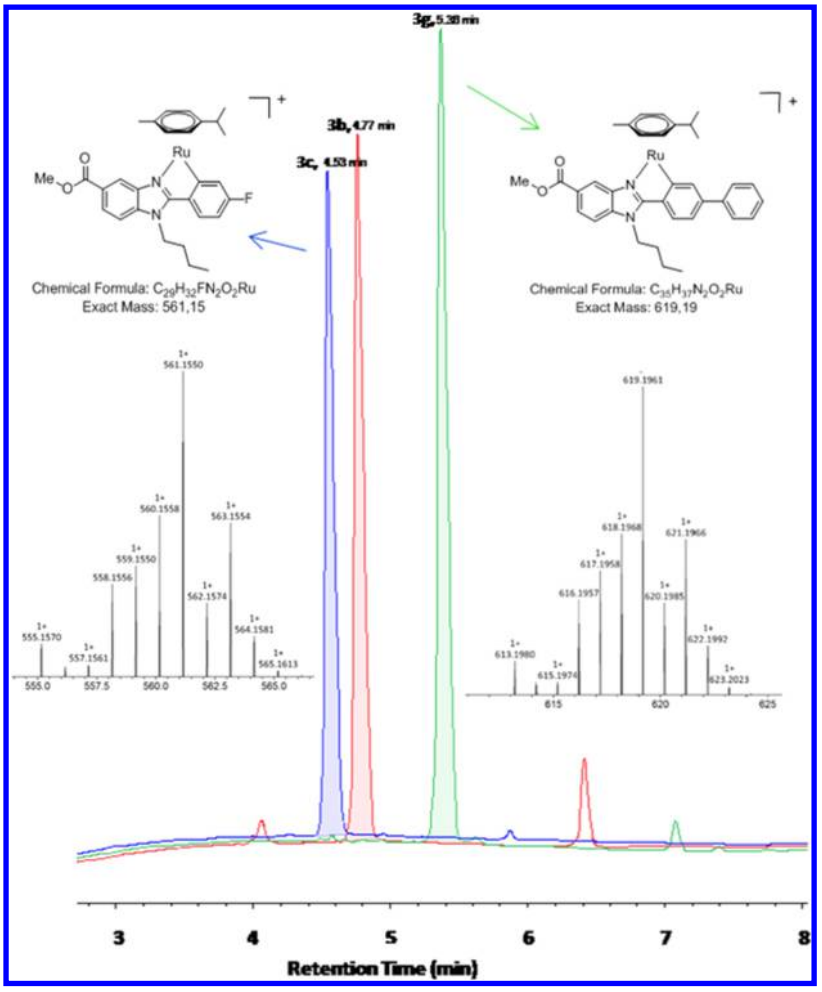


**Figure 5.** RP-UPLC chromatograms with UV detection at 320 nm of 10 $\mu$M **3b,c,g** solutions in mobile phase. Mass spectra for UPLC fractions are also shown for **3c** and **3g**. An Acquity UPLC BEH C18 1.7 $\mu$m particle size analytical column 50 mm × 2.1 mm (Waters) was used. The mobile phases used were A = $H_2O$ with 0.2% HCOOH and B = acetonitrile. The percentage of organic modifier (B) was changed linearly as follows: 0 min, 20%; 1 min, 30%; 8 min, 99%; 8.50 min, 99%; 9.50 min, 20%. Curves were obtained within 4 h after preparation of the **3b,c,g** solutions at room temperature.

**Table 1. $IC_{50}$ ($\mu$M) for 2a, 3a−g, 4a−g, and Cisplatin at 48 h**[a]

| compd | A2780 | A2780cisR | 5637 | A427 | LCLC | SISO | HT29 | EA.hy926 |
|---|---|---|---|---|---|---|---|---|
| **3a** | 1.82 ± 0.35 | 2.37 ± 0.10 | 2.90 ± 0.11 | 2.58 ± 0.64 | 3.52 ± 0.58 | 3.92 ± 0.29 | 2.88 ± 0.55 | 7.05 ± 1.07 |
| **3b** | 1.48 ± 0.35 | 1.46 ± 0.14 | 2.53 ± 0.57 | 2.99 ± 0.24 | 3.50 ± 0.40 | 3.73 ± 0.34 | 3.31 ± 0.04 | 5.49 ± 1.57 |
| **3c** | 1.36 ± 0.07 | 3.26 ± 0.32 | 1.87 ± 0.32 | 1.85 ± 0.29 | 2.16 ± 0.20 | 2.05 ± 0.09 | 2.74 ± 0.11 | >8 |
| **3d** | 1.24 ± 0.45 | 1.98 ± 0.23 | 1.25 ± 0.17 | 1.28 ± 0.07 | 1.41 ± 0.40 | 1.39 ± 0.21 | 1.93 ± 0.07 | 3.35 ± 0.04 |
| **3e** | 1.56 ± 0.48 | 2.18 ± 0.22 | 2.27 ± 0.23 | 1.84 ± 0.60 | 2.45 ± 0.46 | 2.34 ± 0.46 | 2.76 ± 0.31 | 5.10 ± 0.25 |
| **3f** | 1.30 ± 0.45 | 2.52 ± 0.16 | 2.66 ± 0.19 | 1.47 ± 0.18 | 2.32 ± 0.03 | 2.28 ± 2.26 | 2.35 ± 0.27 | 7.21 ± 0.04 |
| **3g** | 1.07 ± 0.34 | 0.96 ± 0.23 | 1.56 ± 0.50 | 1.24 ± 0.07 | 1.31 ± 0.08 | 1.82 ± 0.17 | 1.99 ± 0.08 | 1.67 ± 0.03 |
| **4a** | 1.78 ± 0.85 | 2.59 ± 0.42 | 5.56 ± 0.25 | 3.78 ± 0.41 | 9.86 ± 1.04 | 5.49 ± 0.93 | 1.37 ± 0.38 | 2.85 ± 0.10 |
| **4b** | 3.60 ± 0.28 | 5.65 ± 0.78 | 9.37 ± 0.53 | 7.25 ± 0.28 | 15.14 ± 0.49 | 13.87 ± 0.17 | 8.68 ± 0.92 | >8 |
| **4c** | 2.31 ± 0.39 | 3.37 ± 0.41 | 2.95 ± 0.71 | 4.28 ± 0.55 | 5.58 ± 0.33 | 4.76 ± 0.87 | 9.50 ± 0.75 | 2.99 ± 0.09 |
| **4d** | 2.70 ± 0.13 | 1.93 ± 0.15 | 2.45 ± 0.10 | 2.62 ± 0.56 | 6.63 ± 0.88 | 6.65 ± 0.04 | 3.77 ± 0.31 | 5.22 ± 0.88 |
| **4e** | 2.78 ± 0.12 | 1.70 ± 0.38 | 3.70 ± 0.09 | 2.35 ± 0.62 | 5.10 ± 0.33 | 3.42 ± 0.26 | 6.27 ± 0.69 | 1.19 ± 0.05 |
| **4f** | 2.29 ± 0.46 | 3.76 ± 0.64 | 5.15 ± 0.12 | 2.34 ± 0.06 | 3.47 ± 0.13 | 3.61 ± 0.93 | 5.73 ± 0.43 | 1.98 ± 0.40 |
| **4g** | 1.22 ± 0.41 | 1.21 ± 0.48 | 1.48 ± 0.88 | 1.59 ± 0.34 | 3.61 ± 0.21 | 3.79 ± 0.31 | 4.01 ± 0.56 | 5.95 ± 0.92 |
| **2a** | >15 | >15 | >20 | >50 | >20 | >20 | >25 | >15 |
| CDDP | 1.90 ± 0.20 | 19.57 ± 1.82 | 3.39 ± 0.05 | 6.09 ± 1.49 | 1.92 ± 0.54 | 0.98 ± 0.07 | 7 ± 0.07 | 9.86 ± 0.64 |

[a]Results are averages ± standard errors deviations of three independent experiments.

were dissolved in DMF first and then serially diluted in complete culture medium such that the effective DMF content did not exceed 0.4%, as previously described.[66] CDDP, diluted in water, was used as positive control. Table 1 reports the $IC_{50}$ values of the compounds. On the other hand, $IC_{50}$ values for **3a−g** and **4a−g** in the human umbilical vein endothelial



DOI: 10.1021/acs.jmedchem.5b01194
J. Med. Chem. 2015, 58, 7310−7327

EA.hy926 cell line were also calculated (Table 1) with the aim to verify that the antiangiogenic effect (vide infra) was not due to a cytotoxic effect but rather to their antiangiogenic potential.

The cell growth inhibitory potency of all the metal complexes was noticeably much higher than their parent ligands (e.g., compared with **2a**). Most of the complexes were even more active than CDDP in A427 and HT29 cell lines. As depicted in Table 1, we investigated the effect of H, Me, F, $CF_3$, MeO, $NO_2$, and Ph substituents in the $R_4$ position of the phenyl ring of the 2-phenylbenzimidazole chelating ligand of the ruthenium (**3a**–**g**) and iridium complexes (**4a**–**g**) on the cytotoxicity. Methyl substitution produces no effect on potency compared to the unsubstituted compound (**3a**) in ruthenium series, but it loses some potency in iridium complexes for most of the cell lines. The "magic" fluoro influence was observed with both Ru and Ir complexes, where activity of fluoro-substituted complex was enhanced somewhat in all studied cell lines except the HT29 cell line for iridium **4c**. Trifluoromethyl substitution enhances the activity of Ru complex **3d** in almost all the cell lines, while for the iridium complex **4d** there was no effect on potency in LCLC, SISO, and HT29 cell lines. Activity enhances by electron donating methoxy substitution in A427, LCLC, and SISO cell lines for the ruthenium complex **3e**. Similarly, electron donating nitro substitution also increases potency of **3f** in A427, LCLC, and SISO cell lines as compared to the parent ruthenium complex **3a**, while it shows mixed behavior in the iridium complexes with respect to all cell lines. Certainly no ample discrepancy was detected with donating electronic effect as compared with withdrawing electronic effect in ruthenium complexes taking into account all studied cancer cell lines. Interestingly, phenyl substitution shows increased potency in both Ru and Ir complexes (**3g** and **4g**, respectively) as compared to their parent compounds in all cell lines. In general, ruthenium complexes are more active than the corresponding iridium complexes.

*2.2.2. Complexes **3a**–**g** and **4a**–**g** Overcome the Acquired Resistance to CDDP.* As it is well-known, A2780cisR encompasses all of the known major mechanisms of resistance to cisplatin:[67] reductions in intracellular of drug levels, enhanced DNA repair and/or increased damage tolerance, elevated cellular thiol (GSH) level, and failure of cell-death pathways. The ability of the compound to overcome the acquired resistance to cisplatin was determined from the resistance factor, RF, defined as the ratio between the $IC_{50}$ values of the resistant and the sensitive lines. An RF of <2 is considered as the limit beyond which the compound denotes non-cross-resistance.[68] In general, all the new compounds studied here are able to overcome cisplatin resistance; their RFs are much lower than the RF of cisplatin (Figure 6). As it has been recently shown by using a tracer technique, the ruthenium complex **3a** is able to reduce the uptake and increase the release of the organic osmolyte taurine in Ehrlich Lettré Ascites (ELA) cells, with innate resistance to CDDP, and in A2780 human ovarian cancer cells.[50]

*2.2.3. Accumulation Studies.* The cellular accumulation of the Ru(II) complexes **3b**,**c**,**g** in the A2780 ovarian cancer cell lines was studied to investigate the possible relationship between cellular uptake and cytotoxicity. Cellular concentrations were determined by AAS after 24 h of exposure to **3b**, **3c**, and **3g** at 2 $\mu$M. The results are summarized in Figure 7. As shown, for these compounds a direct relationship between cellular-ruthenium accumulation in A2780 ovarian cells and cytotoxicity is not observed.

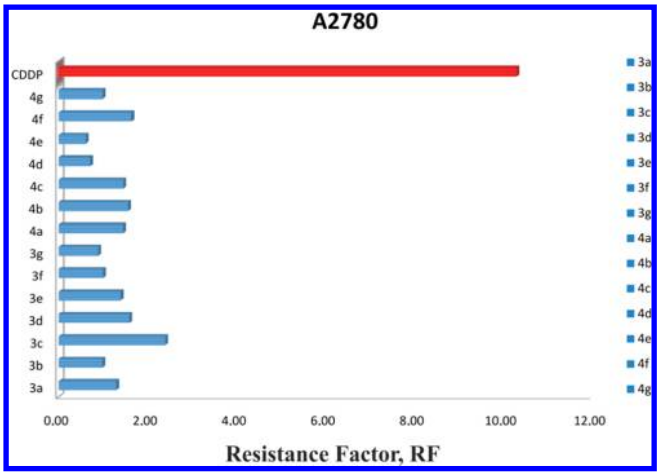


**Figure 6.** Resistance factors, RF, for CDDP and all the complexes studied toward CDDP-resistant A2780 human ovarian cancer cells, A2780cisR.

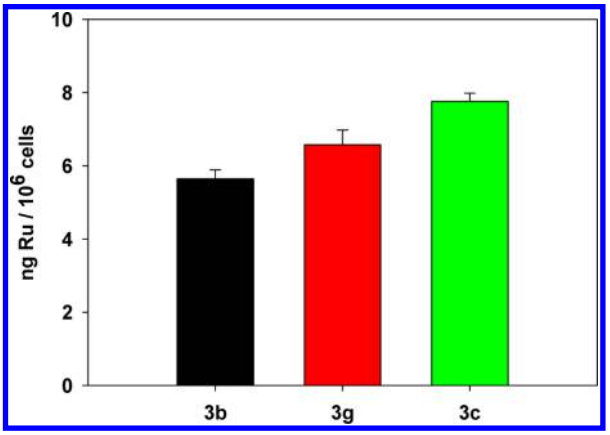


**Figure 7.** Intracellular ruthenium accumulation in A2780 cells at 24 h incubation with complexes **3b**, **3c**, and **3g**. Experiments were made in triplicate.

*2.2.4. DNA-Bound Metal in Cells.* Iridium and ruthenium levels on nuclear DNA were determined after the exposure of A2780 cells to 2 $\mu$M complexes **3g** and **4g** for 24 h. The iridium content of nuclear DNA extracted from the A2780 cells treated with **4g** was found to be 0.74 ± 0.05 pg of Ir per ng of DNA, which is a very small value compared to that of the iridium complex $[(\eta^5\text{-}C_5Me_4C_6H_4C_6H_5)Ir(phen)Cl]^+$ (phen = phenanthroline), which has been shown to cause both nuclear DNA damage and mitochondrial dysfunction in ovarian cancer cells.[69] The ruthenium content of nuclear DNA extracted from the A2780 cells treated with **3g** was found to be also low (1.1 ± 0.09 pg of Ru per ng of DNA), a result that agrees with the intracellular distribution observed for the ruthenium parent compound **3a** in Ehrlich Lettré Ascites (ELA) cells, with an elevated content of **3a** in the cytosol (78%) compared to nuclei and mitochondria.[50]

*2.2.5. Apoptosis Studies.* Apoptotic studies of ruthenium complexes **3d** and **3f** and iridium complexes **4d** and **4f** were carried out with 5637 and SISO cell lines. Exposure of phosphatidylserine (PS) to the outer side of the cell membrane, an early sign of apoptosis, was followed by a flow cytometric assay based on the annexin V-FLUOS, propidium iodide (PI) method, which also can identify necrotic or late apoptotic cells. The results are shown in Figure 8. The four typical quadrants


DOI: 10.1021/acs.jmedchem.5b01194
J. Med. Chem. 2015, 58, 7310–7327

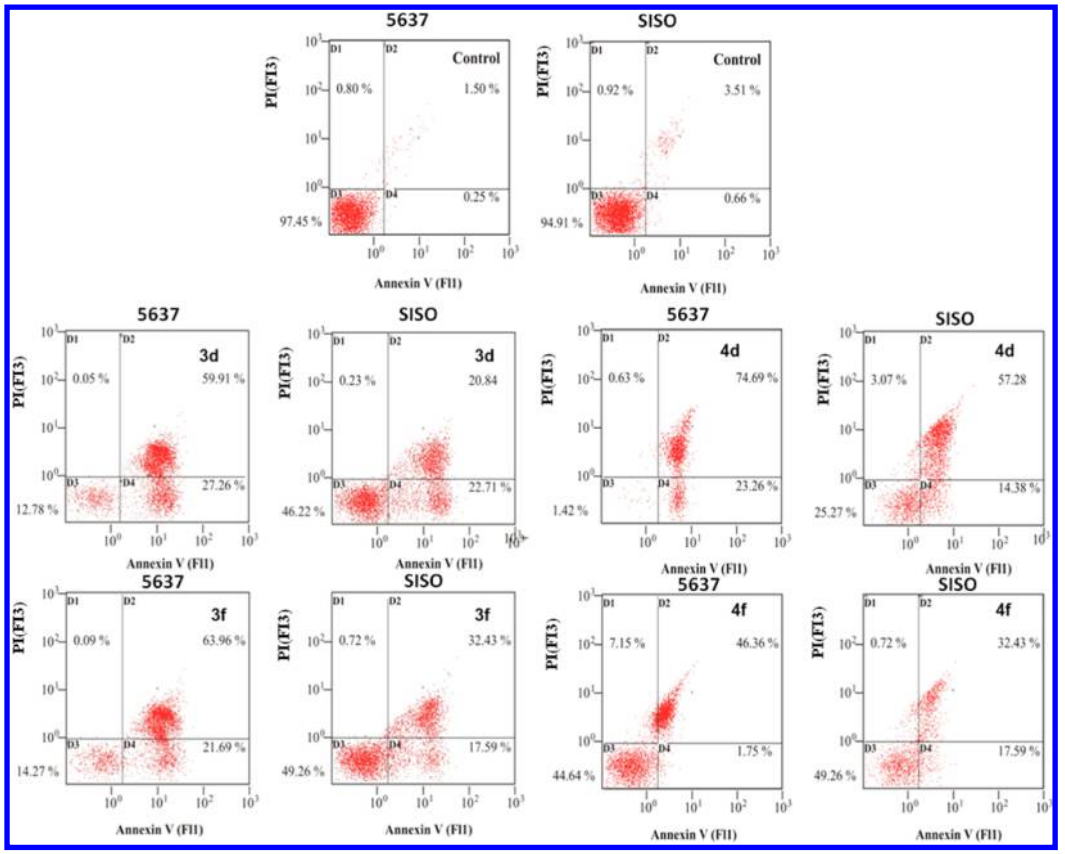


**Figure 8.** Flow cytometry analysis of 5637 and SISO cancer cells after treatment with **3d**, **3f**, **4d**, and **4f** as detected by annexin V/PI. Density plots for untreated cells (control) and for cells treated with 5 $\mu$M (24 h) **3d**, **3f**, **4d** and **4f** are shown. The experiments were performed in triplicate.

identifying the living (lower left quadrant D3, not stained cells), the early apoptotic (lower right quadrant D4, only the annexin-V stained cells), the necrotic (upper left quadrant D1, only PI stained cells), and the late apoptotic (upper right quadrant D2, cells stained with both fluorescent dyes) cells appear in these diagrams. As depicted in Figure 8, it is clear that complexes **3d**, **3f**, **4d**, and **4f** all induce a high incidence of early to late stage apoptosis in both 5637 and SISO cells at 24 h without increasing necrotic population.

*2.2.6. Enhanced Activation of Caspase 3 by Complexes **3a,d** and **4a,d**.* Caspases, in general, are a family of cysteine proteases that play essential roles in apoptosis, necrosis, and inflammation.[70] Colorimetric methods can be used to measure its activation when the DEVD sequence is labeled with p-NA.[71] As shown in Figure 9, complexes **3a,d** and **4a,d** increased caspase-3 activity in A2780 cells (monitored spectrophotometrically using the substrate DEVD-pNA).

*2.2.7. Cell Cycle Arrest.* To understand the effect of complexes **3d** and **3f** on cell growth, their effect on the cell cycle by FACS (fluorescence activated cell sorter) analysis in 5637 and SISO cancer cells was examined. After treatment of 5637 cell lines with 5 $\mu$M **3d** and **3f** for 24 h (Figure 10 and Supporting Information, Figure S10) we found different behaviors of compounds within the same as well as different cell lines. Compound **3d** arrests the cycle in the G2/M phase in both cell lines. However, complex **3f** arrests the cell cycle in the G0/G1 phase of 5637 cells but arrests the cell cycle in G2/M phase in the SISO cell line.

*2.2.8. Intracellular Reactive Oxygen Species (ROS) Determination.* 2′,7′-Dichlorodihydrofluorescein diacetate (DCFH-DA) was used to measure the effect of **3g** and **4g**

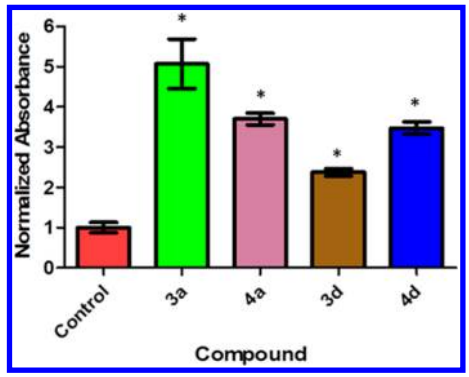


**Figure 9.** Caspase-3 activation in A2780 ovarian cancer cells caused by 24 h exposure to complexes **3a,d** and **4a,d** at 37 °C. Results are expressed as absorbance at 410 nm (detection of *p*-nitroaniline after cleavage from the labeled substrate DEVD-pNA). Concentrations of the complexes used were 2 $\mu$M: (Cont) control cells not treated; (*) $p < 0.05$ was considered to be statistically significant.

and, for comparative purposes, also of cisplatin on the production of ROS by A2780 cells. The DCFH-DA method is designed to provide a highly sensitive, quantifiable, real-time assessment of ROS production.[69,72,73] To evaluate ROS formation, A2780 cells untreated or treated with **3g**, **4g**, or cisplatin were incubated with 25 $\mu$M DCFH-DA for 30 min in the dark. DCFH-DA is cleaved by cellular esterases, oxidized by ROS, and yields a fluorescent product. After incubation, the resulting fluorescence was measured and the data are plotted in Figure 11. Treatment of A2780 cells with **4g** at 2 $\mu$M resulted


DOI: 10.1021/acs.jmedchem.5b01194
J. Med. Chem. 2015, 58, 7310−7327

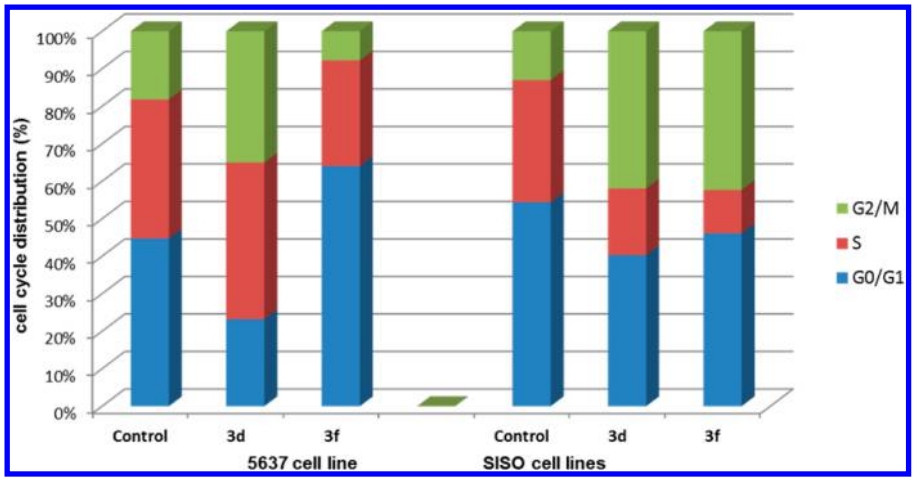


**Figure 10.** Cell cycle analysis of 5637 and SISO cancer cells after 24 h treatment with 1 $\mu$M compounds **3d** and **3f** at 37 °C.

in an increase of fluorescence, indicating the production of ROS.

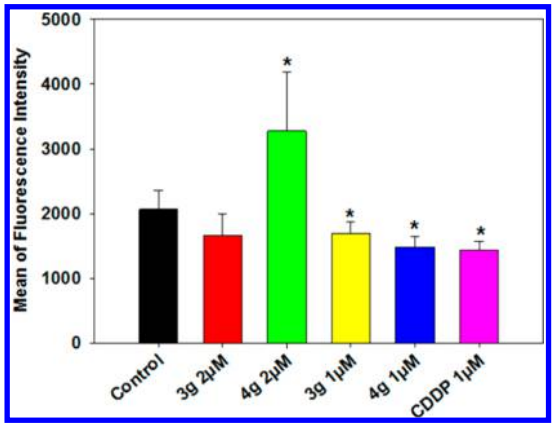


**Figure 11.** Generation of ROS in A2780 cells induced by various concentrations of **3g**, **4g**, or cisplatin at concentrations of one ROS **3g**, **4g**, and cisplatin: (*) $p < 0.05$ was considered to be statistically significant. Experiments were made in triplicate.

**2.3. Interaction with Biomacromolecules.** *2.3.1. Interaction of Ruthenium Complex **3d** with HSA.* Reactions of anticancer metallodrugs with proteins are of considerable interest, as these interactions might feature processes that are crucial for the biodistribution, the toxicity, and even the mechanism of action. HSA is the most abundant of the blood serum proteins and serves as a transport vehicle for a wide variety of ligands, including metal ions and various pharmaceuticals.[32,74−77] It comprises a single chain with 585 amino acids, including a single tryptophan residue (Trp 214) responsible for most of the intrinsic fluorescence of the protein. Upon excitation at 295 nm, HSA strongly fluoresces at $\lambda$ = 350 nm, which can be attenuated by binding of a small molecule at or near local tryptophan environment. The HSA emission spectra in the presence of different concentrations of the benzimidazole complexes were recorded in the wavelength range 300−580 nm by exciting at 295 nm. As seen in Figure 12A, the fluorescence intensities of the protein are increasingly decreased with the increasing concentration of the probed compound, indicating the binding of the complex to the protein. Furthermore, the fluorescence quenching mechanism can be described by the Stern−Volmer equation (eq 1),[78] where $F_0$ and $F$ represent the fluorescence intensities in the

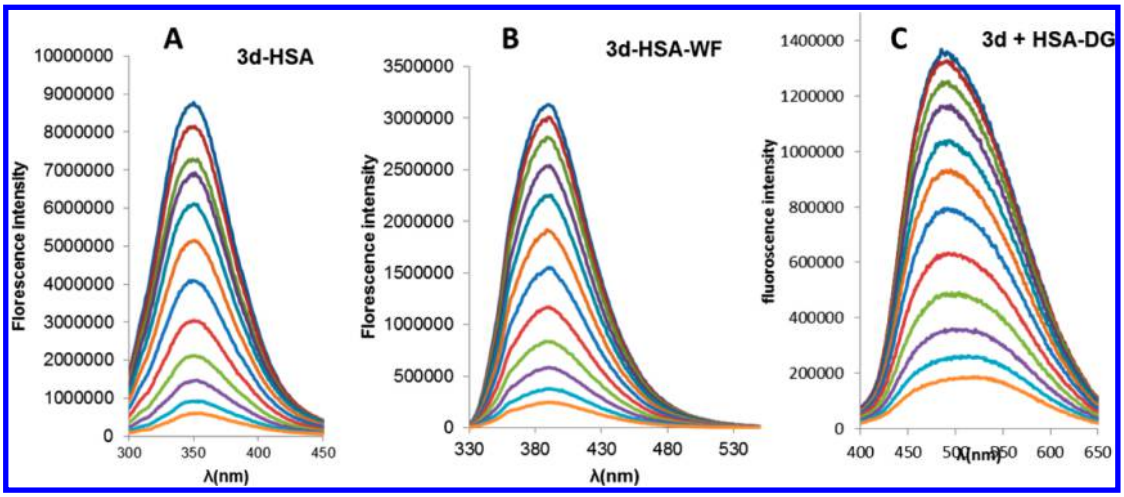


**Figure 12.** Emission spectra of HSA, HSA−WF, and HSA−DG in the presence of increasing amounts of complex **3d**. $\lambda_{ex}$ = 295 nm, [HSA] = 5.0 $\mu$M; $\lambda_{ex}$ = 320 nm, [HSA−WF] = 5.0:5.0 $\mu$M; $\lambda_{ex}$ = 320 nm, [HSA−DG] = 5.0:5.0 $\mu$M; [Complex **3d**]: 0−50 $\mu$M (top to bottom gradual increments). Temperature = 296 K. pH 7.4.



DOI: 10.1021/acs.jmedchem.5b01194
J. Med. Chem. 2015, 58, 7310−7327

absence and the presence of a quencher at a given quencher concentration, respectively. $K_{SV}$ and [Q] are the Stern−Volmer quenching constant, and the quencher concentration, respectively.

$$F_0/F = 1 + K_{SV}[Q] \quad (1)$$

For a homogeneously emitting solution eq 1 predicts a linear plot of $F_0/F$ vs [Q] (Table 2 and Supporting Information, Figure S11).

**Table 2. Quenching and Binding Parameters for the Interaction of Complex 3d with HSA, HSA−WF, and HSA−DG at 298 K**

| study | $10^{-4}K_{SV}$ ($M^{-1}$) | $R$ | $10^{-4}K_A$ ($M^{-1}$) | $n$ |
|---|---|---|---|---|
| HSA | 3.33 | 0.9979 | 6.46 | 1.13 |
| HSA−WF | 3.85 | 0.9989 | 5.69 | 1.54 |
| HSA−DG | 2.82 | 0.9808 | 4.14 | 1.38 |

For a static quenching process, the association constant ($K_A$) and the number of binding sites ($n$) can be calculated using eq 2.

$$\log\frac{F_0 - F}{F} = n\log K_A - n\log\left\{\frac{1}{[Q_t] - (F_0 - F)[P_t]/F_0}\right\} \quad (2)$$

Here $F_0$ and $F$ are the fluorescence intensities in the absence and presence of complexes, respectively; $[Q_t]$ and $[P_t]$ are the total concentrations of complexes and HSA, respectively. Supporting Information, Figure S12 shows the plots of $\log[(F_0 - F)/F]$ versus $\log\{1/([Q_t] - (F_0 - F)[P_t]/F_0)\}$ for the interaction between HSA and complex **3d**. $K_A$ and $n$ obtained from the plots and $K_{SV}$ are listed in Table 2.

*2.3.2. Site-Selective Binding of Complex **3d** on HSA.* There is growing interest in the nature of binding of metallodrugs to biomolecules in order to improved the design of next-generation drug candidates. To identify the binding site location of benzimidazole metal complexes on the region of HSA, competitive binding experiments were carried out by using warfarin (WF), a characteristic marker for site I and dansyl glycine (DG) as one for site II.[79] The weak warfarin fluorescence is enhanced upon binding with HSA because of its interaction with Trp214 in HSA when excited at $\lambda$ = 320 nm. Likewise, the fluorescence of warfarin in its bound state to HSA decreases if a second ligand competes for the same site. Complex **3d** binding site has been evaluated by monitoring the changes in the fluorescence spectra as a function of the gradual increase in complex **3d** concentration in an HSA−WF-complex solution. Figure 12B depicts a decrease in the emission intensity of warfarin when complex **3d** is added. The quenching of warfarin reflects a release of warfarin from HSA; i.e, both warfarin and complex **3d** compete for the same binding site. Therefore, we conclude that **3d** binding occurs at least in part at the warfarin site I. Similarly, a regular decrease in the HAS−DG fluorescence when complex **3d** concentrations are increased also indicates the binding of complex to the protein at the dansyl glycine site II (Figure 12C).

*2.3.3. Hoechst 33258 Displacement from DNA by Ruthenium Complex **3d**.* In order to clarify the binding mode between the new metal complexes and DNA, a fluorescence competition experiment with Hoechst 33258 was employed. This ligand is able to bind via electrostatic interactions to the minor groove of duplex DNA (with marked preference for AT-rich regions) at high DNA/Hoechst ratio.[80] Because of the fluorescence yield of Hoechst 33258 increasing significantly in the presence of DNA, an intensity reduction with complexes addition is interpreted as the displacement of Hoechst bound to ct-DNA. When complex **3d** is added to a Hoechst-DNA solution, a decrease (~81%) is observed in the fluorescence as shown in Figure 13 and Supporting Information (Figure S13). This suggests that complex **3d** is capable of weakly binding to the minor groove of DNA.

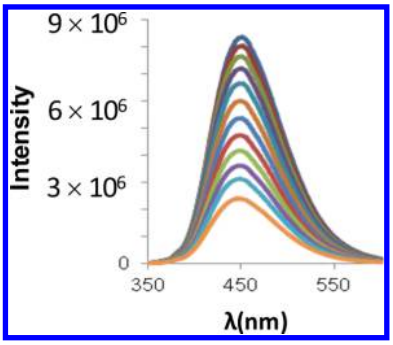


**Figure 13.** Changes in fluorescence spectra of Hoechst−ctDNA in the presence of increasing amounts of complex **3d**. $\lambda_{ex}$ = 450 nm, [DNA] = 10 $\mu$M. [Complex **3d**]: 0−150 $\mu$M (top to bottom gradual increments), 296 K.

**2.4. Inhibition of Tube Formation by Benzimidazole Metal Complexes in EA.hy926 Endothelial Cells.** Angiogenesis is often assessed by the ability of endothelial cells to sprout, migrate, and form vascular tubes in vitro on Matrigel matrix, a gelatinous protein mixture secreted by Engelbreth−Holm−Swarm (EHS) mouse sarcoma cells.[37,81]

In vitro angiogenesis was measured 16 h after incubating EA.hy926 cells with compounds **3a−g** and **4a−g** at concentrations 0.5 $\mu$M (Figure 14). The low concentration was used in order to work at its subcytotoxic concentration in EA.hy926 endothelial cells (Table 1). The resulting formation or inhibition of capillary-like structures was quantified (Figure 14a) by using a combination of the three most representative parameters: total length ($\mu$m), number of meshes (network or polygonal structures), and total meshes area (area occupied by the meshes, $\mu m^2$). Only those compounds that gave significant differences in all the studied parameters were considered antiangiogenic.[45] At 0.5 $\mu$M all complexes inhibit the formation of vascular tubes. Compounds **3d** and **3g** are the most active angiogenic inhibitors in EA.hy926 cells at subcytotoxic concentrations, and at the same time they are also strongly cytotoxic in the assayed cancer cell lines (Table 1). Thus, we conclude that **3d** and **3g** are dual cytotoxic and antiangiogenic compounds.

## 3. CONCLUSIONS

We achieved a successful divergent synthesis of novel C,N-cyclometalated benzimidazole ruthenium(II) and iridium(III) complexes of the types [($\eta^6$-*p*-cymene)RuCl($\kappa^2$-*N*,C-L)] and [($\eta^5$-$C_5Me_5$)IrCl($\kappa^2$-*N*,C-L)] (HL = modified 2-arylbenzimidazole) with various substituents (H, Me, F, $CF_3$, MeO, $NO_2$, and Ph) in the $R_4$ position of the phenyl ring of the 2-phenylbenzimidazole chelating ligand of the ruthenium (**3a−g**) and iridium complexes (**4a−g**). Hydrolysis of the


DOI: 10.1021/acs.jmedchem.5b01194
J. Med. Chem. 2015, 58, 7310−7327

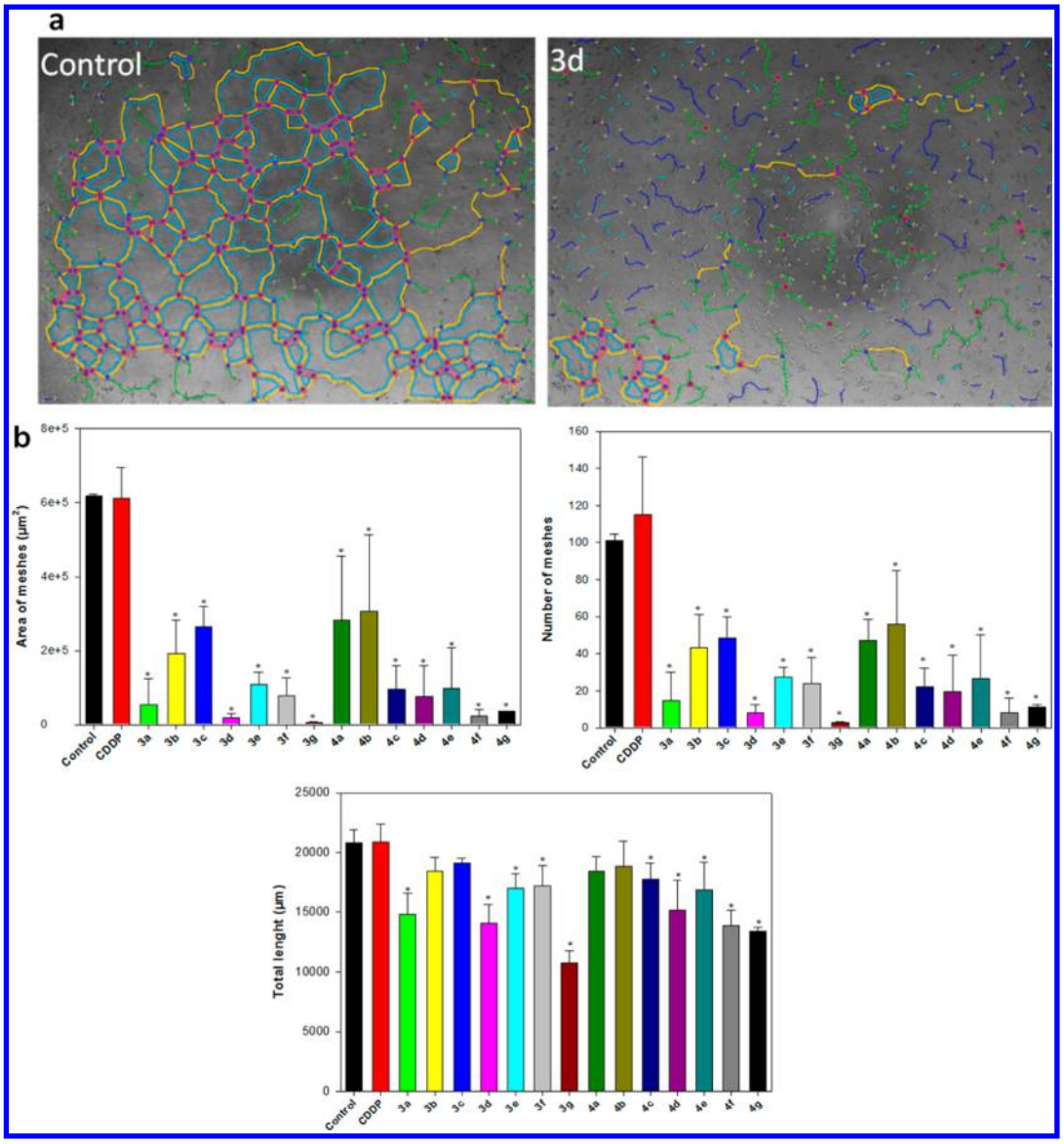


**Figure 14.** Effect of the benzimidazole metal complexes in the endothelial cell tube formation assay. (a) Typical images after an ImageJ process of EA.hy926 cells added to 24-well plates precoated with Matrigel for 16 h: for culture medium as a control and with **3d**, 0.5 $\mu$M. Tube formation of EA.hy926 cells was photographed under an inverted phase-contrast microscope. (b) Quantification after the ImageJ process of number of meshes, total meshes area, and total length of the tubular structure of EA.hy926 cells under 0.5 $\mu$M compounds **3a**−**g** and **4a**−**g** and CDDP for 16 h. Error bars represent the standard deviation of three independent experiments: (∗) $p < 0.05$ was considered to be statistically significant.

ruthenium−chlorido bond is relatively rapid as observed in **3b**,**c**,**g** by $^1$H NMR in MeOD-$d_4$ (containing adventitious water) and 25% MeOD-$d_4$/75% $D_2O$ (v/v) at 37 °C. The cytotoxic activity of the new ruthenium(II) and iridium(III) compounds has been evaluated in a panel of human cancer cell lines (A2780, A427, 5637, LCLC, SISO, and HT29) in order to establish a structure−activity relationship in these families of compounds. Most of the new compounds are more active than CDDP in A427 and HT29 cell lines. Phenyl substitution shows increased potency in both Ru and Ir complexes (**3g** and **4g**, respectively) as compared to their parent compounds in all cell lines. The relative hydrophobicities, according to RP-UPLC−QTOF-MS studies, follow the sequence **3c** < **3b** < **3g**. In general, ruthenium complexes are more active than the corresponding iridium complexes. The new ruthenium and iridium compounds increased caspase-3 activity in A2780 cells, as shown for **3a**,**d** and **4a**,**d**. Furthermore, all the new compounds are able to overcome the cisplatin resistance in A2780cisR cells. Compound **4g** is able to increase the production of ROS in A2780 cells at 2 $\mu$M. The metal content of nuclear DNA extracted from the A2780 cells treated with **3g** and **4g** was found to be low. In addition, some of the metal complexes effectively inhibit angiogenesis in the human umbilical vein endothelial cell line EA.hy926 at 0.5 $\mu$M, with the ruthenium derivatives **3g** (Ph) and **3d** ($CF_3$) being the best inhibitors. Tube formation in EA.hy926, as quantified with the ImageJ software, has also been observed. QC calculations performed on ruthenium model complexes **3′a**,**b**,**d** showed only moderate or slight electron depletion at the phenyl ring of the C,N-cyclometalated ligand and the chlorine atom on increasing the electron withdrawing effect of the R substituent, which explains the little influence observed in activities upon peripheral substitution at the C,N-cyclometalated ligand. Complex **3d** is also capable of weakly binding to the minor


DOI: 10.1021/acs.jmedchem.5b01194
J. Med. Chem. 2015, 58, 7310−7327

groove of DNA and interacts with HSA at both the warfarin site I and dansyl glycine site II. Thus, these novel Ru(II) and Ir(III) organometallic compounds possess a variety of interesting biological effects that make them attractive as potential anticancer drugs.

## 4. EXPERIMENTAL SECTION

**General Methods and Starting Materials.** The C, H, and N analyses were performed with a Carlo Erba model EA 1108 microanalyzer. The $^{1}$H, $^{13}$C, and $^{19}$F spectra were recorded on a Bruker AC 300E, Bruker AV 400, or Bruker AV 600 NMR spectrometer. Chemical shifts are cited relative to $SiMe_4$ ($^{1}$H and $^{13}$C, external) and $CFCl_3$ ($^{19}$F, external). ESI mass (positive mode) analyses were performed on a HPLC/MS TOF 6220. The isotopic distribution of the heaviest set of peaks matched very closely that calculated for the formulation of the complex cation in every case. UV/vis spectroscopy was carried out on a PerkinElmer Lambda 750 S spectrometer with operating software. Fluorescence measurements were carried out with a PerkinElmer LS 55 50 Hz fluorescence spectrometer.

All synthetic manipulations were carried out under an atmosphere of dry, oxygen-free nitrogen using standard Schlenk techniques. Solvents were dried by the usual methods. $[(\eta^6\text{-}p\text{-Cymene})RuCl_2]_2$, $[(\eta^5\text{-}C_5Me_5)IrCl_2]_2$, substituted benzaldehydes, trifluoroacetic acid, magnesium sulfate, sodium sulfate, sodium salt of calf thymus DNA, ethidium bromide (EB), Hoechst 33258, and human serum albumin (HSA) were obtained from Sigma-Aldrich (Madrid, Spain). Deuterated solvents were obtained from Euriso-top. The purity of all biologically evaluated molecules, based on elemental analysis, is >95%.

**Preparation of Compound 1.** 4-Chloro-3-nitrobenzoic acid was dissolved in methanol. Concentrated $H_2SO_4$ (1 mL) was added dropwise in reaction mixture. The reaction mixture was refluxed overnight (18 h), allowed to cool, and then concentrated in vacuo. The resulting residue was dissolved in ethyl acetate and washed with saturated sodium bicarbonate solution. The organic layer was then dried over sodium sulfate and concentrated in vacuo to give the product as white solid.

Methyl 4-chloro-3-nitrobenzoate (1 mmol) was dissolved in dichloromethane (10 mL) in round-bottom flask equipped with stirrer and nitrogen atmosphere. Butylamine (2 mmol) was added to it at room temperature with constant stirring followed by addition of triethylamine (2 mmol). The reaction mixture was stirred at room temperature for 12 h, and the progress of reaction was monitored by TLC. After complete conversion, reaction was quenched by water (10 mL) and product was extracted by dichloromethane (2 × 10 mL). The combined dichloromethane layer was washed with water (10 mL) and brine (10 mL), dried on sodium sulfate, and concentrated under reduced pressure. The crude product was purified by column chromatography using ethyl acetate−hexane (1:5) as eluent to get methyl 4-(butylamino)-3-nitrobenzoate in 79% yield. Subsequently, methyl 4-(butylamino)-3-nitrobenzoate (1 mmol) was dissolved in methanol (10 mL) in a round-bottom flask equipped with stirrer and nitrogen atmosphere. Zinc (3 mmol) was added at room temperature with constant stirring followed by addition of ammonium format (2 mmol) in two batches. The reaction mixture was stirred at room temperature for 5 h, and the progress of reaction was monitored by TLC. After complete conversion, reaction was filtered to remove zinc and unreacted ammonium formate. Filtrate was concentrated and then dissolved in dichloromethane and stirred for 30 min. The undissolved material was removed by filtration, and dichloromethane was concentrated under reduced pressure. The crude product was purified by column chromatography using ethyl acetate−hexane (1:2) as eluent to get methyl 3-amino-4-(butylamino)benzoate (**1**) in 68% yield.

**General Procedure for the Synthesis of Ligands 2a−g.** Methyl 3-amino-4-(butylamino)benzoate **1** (1 mmol) was dissolved in ethanol (10 mL) in a round-bottom flask equipped with stirrer and nitrogen atmosphere. Respective benzaldehyde (1.2 mmol) was added at room temperature with constant stirring followed by addition of trifluoroacetic acid (0.1 mmol) and magnesium sulfate (5 mmol). The reaction mixture was stirred at room temperature for 24 h, and the progress of reaction was monitored by TLC. After complete conversion, reaction was filtered to remove magnesium sulfate. Filtrate was concentrated and then dissolved in dichloromethane. Dichloromethane was washed with water (2 × 10 mL) and brine (10 mL), dried on sodium sulfate, and concentrated under reduced pressure. The crude product was purified by column chromatography using ethyl acetate−hexane (1:3) as eluent to obtain respective ligands (**2a−g**) with good yield.

*Methyl 1-Butyl-2-phenyl-1H-benzimidazole-5-carboxylate,* ***2a.*** White solid. Yield: 57%. Anal. Calcd for **2a** $C_{19}H_{20}N_2O_2$: C, 74.01; H, 6.54; N, 9.08. Found: C, 73.72; H, 6.56; N, 8.77 (%). $^{1}$H NMR (400 MHz, $CDCl_3$): $\delta$ 8.54 (d, 1H, $J$ = 1.4 Hz), 8.06 (dd, 1H, $J$ = 8.5, 1.4 Hz), 7.73 (m, 2H), 7.54 (m, 3H), 7.45 (d, 1H $J$ = 8.5 Hz), 4.26 (t, 2H, $J$ = 7.6 Hz), 3.95 (s, 3H), 1.80 (m, 2H), 1.28 (m, 2H), 0.86 (t, 3H, $J$ = 7.4 Hz). $^{13}$C NMR (100 MHz, $CDCl_3$): $\delta$ 167.6, 155.4, 142.6, 138.8, 130.1, 130.0, 129.2, 128.7, 124.4, 124.1, 122.2, 109.7, 52.0, 44.6, 31.7, 19.8, 13.4. ESI-MS (pos ion mode, $CH_2Cl_2$): $m/z$ 309 ($[M + H]^+$).

*Methyl 1-Butyl-2-(p-tolyl)-1H-benzo[d]imidazole-5-carboxylate,* ***2b.*** Brown orange solid. Yield: 39%. Anal. Calcd for **2b** $C_{20}H_{22}N_2O_2$: C, 74.51; H, 6.88; N, 8.69. Found: C, 74.46; H, 6.77; N, 8.61%. $^{1}$H NMR (400 MHz, $CDCl_3$): $\delta$ 8.52 (d, 1H, $J$ = 1.6 Hz), 8.03 (dd, 1H, $J$ = 8.6, 1.6 Hz), 7.61 (d, 2H, $J$ = 8.1 Hz), 7.42 (d, 1H, $J$ = 8.6 Hz), 7.34 (d, 2H, $J$ = 8.1 Hz), 4.24 (m, 2H), 3.95 (s, 3H), 2.44 (s, 3H), 1.79 (m, 2H), 1.28 (m, 2H), 0.87 (t, 2H, $J$ = 7.3 Hz, 3H). $^{13}$C NMR (100 MHz, $CDCl_3$): $\delta$ 168.5, 156.4, 143.3, 141.2, 139.6, 130.4, 130.0, 127.8, 125.4, 125.1, 122.9, 110.6, 53.0, 45.6, 32.7, 22.4, 20.8, 14.4. ESI-MS (pos ion mode, $CH_2Cl_2$): $m/z$ 323.18 ($[M + H]^+$).

*Methyl 1-Butyl-2-(4-fluorophenyl)-1H-benzo[d]imidazole-5-carboxylate,* ***2c.*** Light orange. Yield: 33%. Anal. Calcd for **2c** $C_{19}H_{19}FN_2O_2$: C, 69.93; H, 5.87; N, 8.58. Found: C, 69.76; H, 5.79; N, 8.57 (%). $^{1}$H NMR (300 MHz, $CDCl_3$): $\delta$ 8.55 (d, 1H, $J$ = 1.6 Hz,), 8.02 (dd, 1H, $J$ = 8.6, 1.6 Hz), 7.69 (m, 2H), 7.40 (d, 1H, $J$ = 8.6 Hz), 7.19 (d, 2H, $J$ = 8.6 Hz), 4.20 (m, 2H), 3.92 (s, 3H), 1.75 (m, 2H), 1.24 (m, 2H), 0.84 (t, $J$ = 7.4 Hz, 3H). $^{13}$C NMR (75 MHz, $CDCl_3$): $\delta$ 167.5, 165.4, 162.1, 154.3, 154.3, 142.2, 138.6, 131.4, 131.3, 126.0, 124.4, 122.1, 116.2, 115.9, 109.8, 52.1, 44.7, 31.8, 19.8, 13.4. $^{19}$F NMR (188 MHz, $CDCl_3$): $\delta$ −109.6. ESI-MS (pos ion mode, $CH_2Cl_2$): $m/z$ 327.15 ($[M + H]^+$).

*Methyl 1-Butyl-2-(4-(trifluoromethyl)phenyl)-1H-benzo[d]-imidazole-5-carboxylate,* ***2d.*** Light brown solid. Yield: 53%. Anal. Calcd for **2d** $C_{20}H_{19}F_3N_2O_2$: C, 63.83; H, 5.09; N, 7.44. Found: C, 63.52; H, 4.97; N, 7.34%. $^{1}$H NMR (300 MHz, $CDCl_3$): $\delta$ 8.54 (d, 1H, $J$ = 1.4 Hz), 8.08 (dd, 1H, $J$ = 8.6, 1.4 Hz), 7.84 (AB quartet, 4H, $J$ = 8.2 Hz), 7.47 (d, 1H, $J$ = 8.6 Hz), 4.26 (m, 2H), 3.96 (s, 3H), 1.81 (m, 2H), 1.28 (m, 2H), 0.88 (t, 3H, $J$ = 7.4 Hz). $^{13}$C NMR (100 MHz, $CDCl_3$) $\delta$ 167.4, 153.6, 142.3, 138.7, 133.5, 129.7, 125.8, 125.8, 125.0, 124.8, 122.4, 122.4, 110.0, 77.2, 52.2, 44.9, 31.9, 19.9, 13, 110.8, 113.55; $^{19}$F NMR (188 MHz, $CDCl_3$): $\delta$ −62.8. ESI-MS (pos ion mode, $CH_2Cl_2$): $m/z$ 377.14 ($[M + H]^+$).

*Methyl 1-Butyl-2-(4-methoxyphenyl)-1H-benzo[d]imidazole-5-carboxylate,* ***2e.*** Yellowish brown solid. Yield: 25%. Anal. Calcd for **2e** $C_{20}H_{22}N_2O_3$: C, 70.99; H, 6.55; N, 8.28. Found: C, 70.90 H, 6.41; N, 8.29%. $^{1}$H NMR (400 MHz, $CDCl_3$): $\delta$ 8.50 (d, 1H, $J$ = 1.4 Hz), 8.02 (dd, 1H, $J$ = 8.4, 1.4 Hz), 7.66 (d, 2H, $J$ = 8.8 Hz), 7.40 (d, 1H, $J$ = 8.4 Hz), 7.04 (d, 2H, $J$ = 8.8 Hz), 4.23 (m, 2H), 3.94 (s, 3H), 3.88 (s, 3H), 1.79 (m, 2H), 1.28 (m, 2H), 0.87 (t, 3H, $J$ = 7.4 Hz). $^{13}$C NMR (100 MHz, $CDCl_3$): $\delta$ 168.5, 161.9, 156.2, 143.3, 139.7, 131.6, 125.3, 125.0, 123.1, 122.8, 115.1, 110.6, 56.3, 53.0, 45.6, 32.7, 20.8, 14.4. ESI-MS (pos ion mode, $CH_2Cl_2$): $m/z$ 339.17 ($[M + H]^+$).

*Methyl 1-Butyl-2-(4-nitrophenyl)-1H-benzo[d]imidazole-5-carboxylate,* ***2f.*** Light brown solid. Yield: 43%. Anal. Calcd for **2f** $C_{19}H_{19}N_3O_4$: C, 64.59; H, 5.42; N, 11.89. Found: C, 64.70; H, 5.31; N, 11.72(%). $^{1}$H NMR (300 MHz, $CDCl_3$): $\delta$ 8.52 (d, 1H, $J$ = 1.0 Hz), 8.39 (d, 2H, $J$ = 8.9 Hz), 8.06 (dd, 1H, $J$ = 8.6, 1.0 Hz), 7.92 (d, 2H, $J$ = 8.9 Hz), 7.45 (d, $J$ = 8.6 Hz, 1H), 4.29 (m, 2H), 3.94 (s, 3H), 1.79 (m, 2H), 1.26 (m, 2H), 0.86 (t, $J$ = 7.3 Hz, 3H). $^{13}$C NMR (75 MHz, $CDCl_3$): $\delta$ 167.3, 152.6, 148.5, 142.6, 138.8, 136.3, 130.2, 125.1,



DOI: 10.1021/acs.jmedchem.5b01194
J. Med. Chem. 2015, 58, 7310−7327

125.0, 124.0, 122.8, 110.0, 52.1, 44.9, 31.8, 19.8, 13.4. ESI-MS (pos ion mode, $CH_2Cl_2$): $m/z$ 354.14 ($[M + H]^+$).

*Methyl 2-([1,1′-Biphenyl]-4-yl)-1-butyl-1H-benzo[d]imidazole-5-carboxylate,* ***2g***. Light gray solid. Yield: 40%. Anal. Calcd for **2g** $C_{25}H_{24}N_2O_2$: C, 78.10; H, 6.29; N, 7.28. Found: C, 77.70; H, 6.14; N, 7.12(%). $^1$H NMR (300 MHz, $CDCl_3$): $\delta$ 8.55 (d, 1H, $J$ = 1.23 Hz), 8.06 (dd, 1H, $J$ = 8.6, 1.2 Hz), 7.79 (AB quartet, 4H, $J$ = 8.4 Hz), 7.67 (d, 2H, $J$ = 8.1 Hz), 7.52−7.39 (m, 4H), 4.30 (m, 2H), 3.99 (s, 3H), 1.84 (m, 2H), 1.32 (m, 2H), 0.90 (t, 3H, $J$ = 7.3 Hz). $^{13}$C NMR (75 MHz, $CDCl_3$): $\delta$ 167.6, 155.1, 142.8, 142.5, 140.0, 138.8, 129.7, 128.9, 128.7, 127.9, 127.4, 127.1, 124.6, 124.3, 122.1, 109.8, 52.1, 44.8, 31.8, 19.9, 13.5. ESI-MS (pos ion mode, $CH_2Cl_2$): $m/z$ 385.19 ($[M + H]^+$).

**General Procedure for the Synthesis of Ruthenium Complexes 3a−g.** The corresponding benzimidazole core ligand **2a−g** (1 mmol) was dissolved in freshly distilled dichloromethane in a dry round-bottom flask equipped with stirrer and nitrogen atmosphere. Sodium acetate (1.2 mmol) was added at room temperature with constant stirring followed by addition of $[(\eta^6\text{-}p\text{-cymene})RuCl_2]_2$ (0.5 mmol). The reaction mixture was stirred at room temperature for 12 h, and the progress of reaction was monitored by TLC. After complete conversion, dichloromethane was removed under reduced pressure and diethyl ether (10 mL) was added in it. The reaction mixture was stirred for 10 min, and product was precipitate out. The crystalline product was filtered through G4 filtration funnel and dried well to obtain the corresponding ruthenium metal complex (**3a−g**).

*Complex* ***3a***. Reddish brown color solid. Yield: 60%. Anal. Calcd for **3a** $C_{29}H_{33}ClN_2O_2Ru$: C, 60.25; H, 5.75; N, 4.84. Found: C, 59.54; H, 5.58; N, 4.75 (%). $^1$H NMR (600 MHz, $CDCl_3$): $\delta$ 8.64 (d, 1H, $J$ = 1.4 Hz), 8.35 (dd, 1H, $J$ = 7.5, 1.0 Hz), 8.03 (dd, 1H, $J$ = 8.5, 1.4 Hz), 7.64 (d, 1H, $J$ = 7.5 Hz), 7.37 (d, 1H, $J$ = 8.5 Hz), 7.23 (dt, 1H, $J$ = 7.5, 1.0 Hz), 7.07 (dt, 1H, $J$ = 7.5, 1.0 Hz), 5.90 (d, 1H, $J$ = 5.9 Hz), 5.74 (d, 1H, $J$ = 5.9 Hz), 5.37 (d, 1H, $J$ = 5.9 Hz), 5.13 (d, 1H, $J$ = 5.9 Hz), 4.48 (m, 1H), 4.37 (m, 1H), 4.02 (s, 3H), 2.31 (m, 1H), 2.10 (s, 3H), 1.90 (m, 2H), 1.44 (m, 2H), 0.95 (t, 3H, $J$ = 7.3 Hz), 0.94 (d, 3H, $J$ = 7.0 Hz), 0.78 (d, 3H, $J$ = 7.0 Hz). $^{13}$C NMR (150 MHz, $CDCl_3$): $\delta$ 184.6, 167.1, 159.5, 140.9, 140.7, 139.2, 133.3, 129.1, 125.2, 124.5, 124.3, 122.6, 119.2, 109.6, 101.2, 99.6, 89.4, 89.1, 82.1, 81.2, 52.2, 44.9, 31.6, 30.8, 22.4, 21.7, 20.1, 18.9, 13.7. ESI-MS (pos ion mode, $CH_2Cl_2$): $m/z$ 579 ($[M + H]^+$).

*Complex* ***3b***. Brown solid. Yield: 50%. Anal. Calcd for **3b** $C_{30}H_{35}ClN_2O_2Ru$: C, 60.85; H, 5.96; N, 4.73. Found: C, 60.30; H, 5.89; N, 4.60 (%). $^1$H NMR (400 MHz, $CDCl_3$): $\delta$ 8.60 (s, 1H), 8.16 (s, 1H), 8.01 (d, 1H, $J$ = 7.7 Hz), 7.53 (d, 1H, $J$ = 7.9 Hz), 7.35 (d, 1H, $J$ = 8.5 Hz), 6.88 (d, 1H, $J$ = 7.9 Hz), 5.88 (d, 1H, $J$ = 5.9 Hz), 5.70 (d, 1H, $J$ = 5.9 Hz), 5.38 (d, 1H, $J$ = 5.9 Hz), 5.10 (d, 1H, $J$ = 5.9 Hz), 4.35 (m, 2H), 3.99 (s, 3H), 2.43 (s, 3H), 2.28 (m, 1H), 2.08 (s, 3H), 1.88 (m, 2H), 1.41 (m, 2H), 0.94 (t, 3H, $J$ = 7.3 Hz), 0.93 (d, 3H, $J$ = 7.0 Hz), 0.78 (d, 3H, $J$ = 7.0 Hz). $^{13}$C NMR (300 MHz, $CDCl_3$): $\delta$ 184.50, 167.19, 159.61, 141.29, 140.97, 139.17, 139.13, 130.50, 124.97, 124.23, 123.95, 123.80, 118.92, 109.45, 101.01, 99.14, 89.19, 89.02, 82.28, 80.94, 52.18, 44.77, 31.56, 30.84, 22.40, 21.85, 21.77, 20.04, 18.89, 13.65. ESI-MS (pos ion mode, $CH_2Cl_2$): $m/z$ 593.15 ($[M + H]^+$).

*Complex* ***3c***. Yellow crystalline solid. Yield: 67%. Anal. Calcd for **3c** $C_{29}H_{32}ClFN_2O_2Ru$: C, 58.43; H, 5.41; N, 4.70. Found: C, 58.58; H, 5.35; N, 4.56 (%). $^1$H NMR (200 MHz, $CDCl_3$): $\delta$ 8.61 (d, 1H, $J$ = 1.4 Hz), 8.07 (m, 2H), 8.03 (m, 1H), 7.64 (m, 1H), 7.40 (d, 1H, $J$ = 8.7 Hz), 6.80 (m, 1H), 5.90 (d, 1H, $J$ = 6.0 Hz), 5.72 (d, 1H, $J$ = 6.0 Hz), 5.40 (d, 1H, $J$ = 6.0 Hz), 5.15 (d, 1H, $J$ = 6.0 Hz), 4.47 (m, 2H), 4.02 (s, 3H), 2.31 (m, 1H), 2.11 (s, 3H), 1.92 (m, 2H), 1.44 (m, 2H), 0.95 (t, 3H, $J$ = 7.3 Hz), 0.94 (d, 3H, $J$ = 7.0 Hz), 0.76 (d, 3H, $J$ = 7.0 Hz). $^{13}$C NMR (400 MHz, $CDCl_3$): $\delta$ 178.40, 168.04, 159.62, 141.77, 140.03, 130.47, 127.65, 126.31, 126.16, 125.45, 121.37, 119.93, 110.63, 100.90, 91.07, 90.26, 90.00, 89.22, 83.43, 82.37, 53.20, 45.71, 32.51, 31.80, 23.33, 22.68, 20.98, 19.83, 14.61 ppm. ESI-MS (pos ion mode, $CH_2Cl_2$): $m/z$ 561.41 ($[M - Cl]^+$).

*Complex* ***3d***. Bright yellow powder solid. Yield: 33%. Anal. Calcd for **3d** $C_{30}H_{32}ClF_3N_2O_2Ru$: C, 55.77; H, 4.99; N, 4.33. Found: C, 55.85; H, 4.93; N, 4.30 (%). $^1$H NMR (200 MHz, $CDCl_3$): $\delta$ 8.64 (d, 1H, $J$ = 1.2 Hz), 8.56 (d, 1H, $J$ = 0.9 Hz), 8.06 (dd, 1H, $J$ = 8.4, 1.2 Hz), 7.69 (d, 1H, $J$ = 8.1 Hz), 7.41 (d, 1H, $J$ = 8.4 Hz), 7.30 (dd, 1H, $J$ = 8.1, 0.9 Hz), 5.92 (d, 1H, $J$ = 5.7 Hz), 5.75 (d, 1H, $J$ = 5.9 Hz), 5.40 (d, 1H, $J$ = 5.9 Hz), 5.16 (d, 1H, $J$ = 5.7 Hz), 4.44 (m, 2H), 4.01 (s, 3H), 2.17 (m, 1H), 2.10 (s, 3H), 1.89 (m, 2H), 1.42 (m, 2H), 0.95 (t, 3H, $J$ = 7.3 Hz), 0.94 (d, 3H, $J$ = 6.9 Hz), 0.76 (d, 3H, $J$ = 6.9 Hz). $^{13}$C NMR (50 MHz, $CDCl_3$): $\delta$ 184.8, 166.9, 158.2, 140.8, 139.0, 136.6, 136.4, 129.7, 129.3, 125.6, 125.0, 123.7, 119.5, 110.0, 101.9, 100.5, 89.6, 89.2, 82.5, 81.3, 77.2, 52.3, 45.0, 31.7, 30.9, 22.4, 21.7, 20.0, 18.9, 13.6. $^{19}$F NMR (188 MHz, $CDCl_3$): $\delta$ −62.1. ESI-MS (pos ion mode, $CH_2Cl_2$): $m/z$ 647.12 ($[M + H]^+$).

*Complex* ***3e***. Greenish yellow powder solid. Yield: 54%. Anal. Calcd for **3e** $C_{30}H_{35}ClN_2O_3Ru$: C, 59.25; H, 5.80; N, 4.61. Found: C, 58.54; H, 5.77; N; 4.51 (%). $^1$H NMR (200 MHz, $CDCl_3$): $\delta$ 8.59 (d, 1H, $J$ = 1.5 Hz), 8.01 (1H, dd, $J$ = 7.5, 1.5 Hz), 7.90 (d, 1H, $J$ = 2.5 Hz), 7.61 (d, 1H, $J$ = 8.6 Hz), 7.35 (d, 1H, $J$ = 8.6 Hz), 6.64 (dd, 1H, $J$ = 7.5, 2.5 Hz), 5.88 (d, 1H, $J$ = 5.7 Hz), 5.72 (d, 1H, $J$ = 5.7 Hz), 5.39 (d, 1H, $J$ = 5.7 Hz), 5.12 (d, 1H, $J$ = 5.7 Hz), 4.40 (m, 2H), 4.02 (s, 3H), 3.94 (s, 3H), 2.34 (m, 1H), 2.10 (s, 3H), 1.89 (m, 2H), 1.44 (m, 2H), 0.97 (t, 3H, $J$ = 7.3 Hz), 0.96 (d, 3H, $J$ = 6.6 Hz), 0.68 (d, 3H, $J$ = 6.6 Hz). $^{13}$C NMR (50 MHz, $CDCl_3$): $\delta$ 186.72, 167.23, 159.38, 159.14, 141.01, 139.21, 126.23, 125.26, 125.16, 124.88, 124.04, 118.61(2C), 109.33, 101.00, 99.37, 89.27, 88.78, 82.24, 81.29, 55.11, 52.17, 44.66, 31.50, 30.82, 22.44, 21.68, 20.04, 18.86, 13.66. ESI-MS (pos ion mode, $CH_2Cl_2$): $m/z$ 609.14 ($[M + H]^+$).

*Complex* ***3f***. Light brown solid. Yield: 35%. Anal. Calcd for **3f** $C_{29}H_{32}ClN_3O_4Ru$: C, 55.90; H, 5.18; N, 6.74. Found: C, 55.48; H, 5.22; N, 6.48 (%). $^1$H NMR (200 MHz, $CDCl_3$): $\delta$ 9.14 (d, 1H, $J$ = 2.2 Hz), 8.69 (d, 1H, $J$ = 1.5 Hz), 8.14 (dd, 1H, $J$ = 8.5, 1.5 Hz), 7.93 (dd, 1H, $J$ = 8.5, 2.2, Hz), 7.77 (d, 1H, $J$ = 8.5 Hz), 7.47 (d, 1H, $J$ = 8.5 Hz), 5.98 (dd, 1H, $J$ = 6.0 Hz), 5.81 (dd, 1H, $J$ = 5.6 Hz), 5.49 (d, 1H, 6.0 Hz), 5.26 (d, 1H, $J$ = 5.6 Hz), 4.55 (m, 2H), 4.03 (s, 3H), 2.25 (m, 1H), 2.15 (s, 3H), 1.94 (m, 2H), 1.49 (m, 2H), 0.98 (t, 3H, $J$ = 7.3 Hz), 0.97 (d, 3H, $J$ = 7.0 Hz), 0.78 (d, 3H, $J$ = 7.0 Hz). ESI-MS (pos ion mode, $CH_2Cl_2$): $m/z$ 588.14 ($[M - Cl]^+$).

*Complex* ***3g***. Gray solid. Yield: 56%. Anal. Calcd for **3g** $C_{35}H_{37}ClN_2O_2Ru$: C, 64.26; H, 5.70; N, 4.28. Found: C, 63.47; H, 5.46, N, 4.17 (%). $^1$H NMR (200 MHz, $CDCl_3$): $\delta$ 8.66 (d, 1H, $J$ = 1.5 Hz), 8.58 (d, 1H, $J$ = 1.8 Hz), 8.02 (dd, 1H, $J$ = 8.6, 1.5 Hz), 7.75 (m, 3H), 7.47 (m, 5H), 5.91 (d, 1H, $J$ = 5.7 Hz), 5.79 (d, 1H, $J$ = 5.9 Hz), 5.40 (d, 1H, $J$ = 5.9 Hz), 5.18 (d, 1H, $J$ = 5.7 Hz), 4.48 (m, 2H), 4.03 (s, 3H), 2.33 (m, 1H), 2.11 (s, 3H), 1.95 (m, 2H), 1.45 (m, 2H), 0.99 (t, 3H, $J$ = 7.3 Hz), 0.98 (d, 3H, $J$ = 6.9 Hz), 0.81 (d, 3H, $J$ = 6.9 Hz). $^{13}$C NMR (50 MHz, $CDCl_3$): $\delta$ 185.73, 168.10, 160.25, 142.47, 142.16, 141.96, 140.18, 139.96, 133.35, 129.56, 128.52(2C), 128.26(2C), 126.11, 125.43, 125.22, 122.95, 120.05, 110.55, 102.00, 100.79, 90.59, 89.83, 83.00, 82.20, 53.18, 45.85, 32.61, 31.84, 23.47, 22.64, 21.04, 19.86, 14.63. ESI-MS (pos ion mode, $CH_2Cl_2$): $m/z$ 619.18 ($[M - Cl]^+$).

**General Procedure for the Synthesis of Iridium Complexes 4a−g.** The corresponding benzimidazole core ligand **2a−g** (1 mmol) was dissolved in freshly distilled dichloromethane in a dry round-bottom flask equipped with stirrer and nitrogen atmosphere. Sodium acetate (1.2 mmol) was added to it at room temperature with constant stirring followed by addition of $[(\eta^5\text{-}C_5Me_5)IrCl_2]_2$ (0.5 mmol). The reaction mixture was stirred at room temperature for 12 h. After complete conversion, dichloromethane was removed under reduced pressure and product was precipitate by addition of diethyl ether (10 mL) with constant stirring. The crystalline product was filtered and dried well to obtain the corresponding iridium metal complex (**4a−g**).

*Complex* ***4a***. Yellow solid. Yield: 87%. Anal. Calcd for **4a** $C_{29}H_{34}ClN_2O_2Ir$: C, 51.97; H, 5.11; N, 4.18. Found: C, 51.84; H, 5.07; N, 4.20 (%). $^1$H NMR (400.13 MHz, $CDCl_3$): $\delta$ 8.44 (d, 1H, $J$ = 1.5 Hz), 8.03 (d, 1H, $J$ = 7.5 Hz), 8.00 (dd, 1H, $J$ = 8.5, 1.5 Hz), 7.67 (d, 1H, $J$ = 7.5 Hz), 7.38 (d, 1H, $J$ = 8.5 Hz), 7.21 (dt, 1H, $J$ = 7.5, 1.0 Hz), 7.08 (dd, 1H, $J$ = 7.5, 1.0 Hz), 4.53 (m, 2H), 3.97 (s, 3H), 1.99 (m, 2H), 1.78 (s, 15H), 1.51 (m, 2H), 1.00 (t, 3H, $J$ = 7.4 Hz). $^{13}$C NMR (100.60 MHz, $CDCl_3$): $\delta$ 167.1, 166.3, 163.6, 139.3, 139.2, 137.1, 133.5, 130.9, 125.1, 124.4, 124.0, 122.0, 119.0, 109.8, 88.3, 52.1,



DOI: 10.1021/acs.jmedchem.5b01194
J. Med. Chem. 2015, 58, 7310−7327

44.9, 31.8, 20.2, 13.7, 9.7. ESI-MS (pos ion mode, $CH_2Cl_2$): $m/z$ 635 ($[M - Cl]^+$).

*Complex* ***4b***. Yellow orange solid. Yield: 83%. Anal. Calcd for **4b** $C_{30}H_{36}ClN_2O_2Ir$: C, 52.66; H, 5.30; N, 4.09. Found: C, 52.79; H, 5.24; N, 3.96 (%). $^1H$ NMR (300 MHz, $CDCl_3$): $\delta$ 8.39 (d, 1H $J$ = 1.5 Hz), 7.97 (dd, 1H, $J$ = 8.6, 1.5 Hz), 7.83 (d, 1H, $J$ = 1.1 Hz), 7.55 (d, 1H, $J$ = 8.0 Hz), 7.33 (d, 1H, $J$ = 8.6 Hz), 6.88 (dd, 1H, $J$ = 8.0, 1.1 Hz), 4.45 (m, 2H), 3.95 (s, 3H), 2.43 (s, 3H), 1.95 (m, 2H), 1.76 (s, 15H), 1.48 (m, 2H), 1.19 (t, 3H, $J$ = 7.1 Hz). $^{13}C$ NMR (75 MHz, $CDCl_3$): $\delta$ 167.1, 166.2, 163.7, 140.8, 139.2, 137.8, 130.8, 124.9, 124.1, 123.7, 123.1, 118.8, 109.6, 88.1, 52.1, 44.8, 31.7, 21.6, 20.1, 13.7, 9.6. ESI-MS (pos ion mode, $CH_2Cl_2$): $m/z$ 649.24 ($[M - Cl]^+$).

*Complex* ***4c***. Yellow solid. Yield: 90%. Anal. Calcd for **4c** $C_{29}H_{33}ClFN_2O_2Ir$: C, 50.61; H, 4.83; N, 4.07. Found: C, 50.47; H; 4.76; N; 4.03 (%). $^1H$ NMR (300 MHz, $CDCl_3$): $\delta$ 8.39 (d, 1H, $J$ = 1.6 Hz), 7.99 (dd, 1H, $J$ = 8.6, 1.6 Hz), 7.65 (m, 2H), 7.35 (d, 1H, $J$ = 8.6 Hz), 6.78 (m, 1H), 4.43 (m, 2H), 3.96 (s, 3H), 1.95 (m, 2H), 1.77 (s, 15H), 1.49 (m, 2H), 0.99 (t, 3H, $J$ = 7.3 Hz). $^{13}C$ NMR (75 MHz, $CDCl_3$): $\delta$ 169.4, 169.4, 167.0, 165.5, 162.6, 162.1, 139.1, 139.0, 129.8, 125.5, 125.4, 125.1, 124.4, 123.1, 122.9, 118.8, 109.8, 109.5, 109.1, 88.4, 65.8, 52.1, 44.8, 31.7, 20.1, 15.2, 13.7, 9.6. ESI-MS (pos ion mode, $CH_2Cl_2$): $m/z$ 653.22 ($[M - Cl]^+$).

*Complex* ***4d***. Yellow crystalline solid. Yield: 57%. Anal. Calcd for **4d** $C_{30}H_{33}ClF_3N_2O_2Ir$: C, 48.81; H, 4.50; N, 3.79. Found: C, 48.56; H; 4.40; N; 3.78(%). $^1H$ NMR (300 MHz, $CDCl_3$): $\delta$ 8.47 (d, 1H, $J$ = 1.4 Hz), 8.27 (d, 1H, $J$ = 1.1 Hz), 8.05 (dd, 1H, $J$ = 8.6, 1.4 Hz), 7.74 (d, 1H, $J$ = 8.1 Hz), 7.42 (d, 1H, $J$ = 8.6 Hz), 7.33 (dd, 1H, $J$ = 8.1, 1.1 Hz), 4.50 (m, 2H), 3.99 (s, 3H), 1.98 (m, 2H), 1.79 (s, 15H), 1.51 (m, 2H), 1.01 (t, 3H, $J$ = 7.3 Hz). $^{13}C$ NMR (75 MHz, $CDCl_3$): $\delta$ 166.9, 166.3, 162.2, 139.1, 139.0, 136.9, 133.2, 131.3, 131.0, 125.6, 125.0, 123.6, 119.4, 119.0, 110.2, 88.7, 77.2, 52.3, 45.1, 31.9, 20.2, 13.7, 9.6. ESI-MS (pos ion mode, $CH_2Cl_2$): $m/z$ 703.21 ($[M - Cl]^+$).

*Complex* ***4e***. Light yellow crystalline solid. Yield: 92%. Anal. Calcd for **4e** $C_{30}H_{36}ClN_2O_3Ir$: C, 51.46; H, 5.18; N, 4.00. Found: C, 51.36; H; 5.22; N; 4.05 (%). $^1H$ NMR (300 MHz, $CDCl_3$): $\delta$ 8.37 (d, 1H, $J$ = 1.5 Hz), 7.96 (dd, 1H, $J$ = 8.7, 1.5 Hz), 7.61 (d, 1H $J$ = 8.7 Hz), 7.56 (d, 1H, $J$ = 2.7 Hz), 7.32 (d, 1H, $J$ = 8.5 Hz), 6.64 (dd, 1H, $J$ = 8.5, 2.7 Hz), 4.43 (m, 2H), 3.95 (s, 3H), 3.91 (s, 3H), 1.95 (m, 2H), 1.77 (s, 15H), 1.49 (m, 3H), 0.99 (t, 3H, $J$ = 7.4 Hz). $^{13}C$ NMR (75 MHz, $CDCl_3$): $\delta$ 167.1, 163.4, 161.0, 139.2, 126.4, 125.2, 124.8, 123.9, 121.3, 118.4, 109.4, 108.8, 88.2, 55.0, 52.1, 44.7, 31.6, 20.2, 13.7, 9.6. ESI-MS (pos ion mode, $CH_2Cl_2$): $m/z$ 665.24 ($[M - Cl]^+$).

*Complex* ***4f***. Light red brick solid. Yield: 64%. Anal. Calcd for **4f** $C_{29}H_{33}ClN_3O_4Ir$: C, 48.70; H, 4.65; N, 5.87. Found: C, 48.77; H; 4.50; N; 5.74(%). $^1H$ NMR (300 MHz, $CDCl_3$): $\delta$ 8.83 (d, 1H, $J$ = 2.3 Hz), 8.47 (d, 1H, $J$ = 1.5 Hz), 8.08 (dd, 1H, $J$ = 8.7, 1.5 Hz), 7.93 (dd, 1H, $J$ = 8.5, 2.3 Hz), 7.76 (d, 1H, $J$ = 8.7 Hz), 7.44 (d, 1H, $J$ = 8.5 Hz), 4.53 (m, 2H), 3.97 (s, 3H), 1.98 (m, 2H), 1.80 (s, 15H), 1.54 (m, 2H), 1.01 (t, 3H, $J$ = 7.4 Hz). $^{13}C$ NMR (75 MHz, $CDCl_3$): $\delta$ 167.2, 166.7, 131.2, 147.9, 139.5, 139.1, 130.7, 125.9, 125.4, 123.7, 119.6, 117.5, 110.3, 89.0, 52.3, 45.2, 31.7, 20.1, 13.6, 9.6. ESI-MS (pos ion mode, $CH_2Cl_2$): $m/z$ 680.21 ($[M - Cl]^+$).

*Complex* ***4g***. Light yellow solid. Yield: 73%. Anal. Calcd for **4g** $C_{35}H_{38}ClN_2O_2Ir$: C, 56.33; H, 5.13 N, 3.75. Found: C, 56.40; H, 5.08; N, 3.70 (%). $^1H$ NMR (300 MHz, $CDCl_3$): $\delta$ 8.45 (d, 1H, $J$ = 1.5 Hz), 8.28 (d, 1H, $J$ = 1.8 Hz), 8.02 (dd, 1H, $J$ = 8.6, 1.5 Hz), 7.73 (m, 3H), 7.47 (m, 5H), 4.52 (m, 2H), 3.98 (s, 3H), 2.02 (m, 2H), 1.82 (s, 15H), 1.02 (t, 3H, $J$ = 7.3 Hz). $^{13}C$ NMR (75 MHz, $CDCl_3$): $\delta$ 167.1, 166.5, 163.4, 142.7, 141.4, 139.3, 139.2, 135.6, 132.7, 128.7, 127.4, 127.3, 125.1, 124.4, 124.2, 121.4, 119.0, 109.8, 88.3, 52.2, 31.8, 20.2, 13.8, 9.8. ESI-MS (pos ion mode, $CH_2Cl_2$): $m/z$ 711.26 ($[M - Cl]^+$).

**X-ray Crystal Structure Analysis.** Single crystals suitable for X-ray diffraction analysis were obtained for complexes **3d** and **4d** from $CH_2Cl_2$/toluene/hexane. A summary of crystal data collection and refinement parameters for all compounds are given in Tables S1–S5 in the Supporting Information. Crystals were mounted on glass fibers and transferred to the cold gas stream of the diffractometer Bruker Smart APEX. Data were recorded with Mo K$\alpha$ radiation ($\lambda$ = 0.710 73 Å) in $\omega$ scan mode. Absorption correction for the compound was based on multiscans.

Both structures were solved by direct methods (SHELXS-97);[82] refinement was done by full-matrix least-squares on $F^2$ using the SHELXL-97 program suite;[82] empirical (multiscan) absorption correction was with SADABS (Bruker).[83] All non-hydrogen positions were refined with anisotropic temperature factors. Hydrogen atoms for aromatic CH, aliphatic $CH_2$, and $CH_3$ groups were positioned geometrically (C–H = 0.95 Å for aromatic CH, C–H = 0.99 Å for $CH_2$, C–H = 0.98 Å for $CH_3$) and refined using a riding model (AFIX 43 for aromatic CH, AFIX 23 for $CH_2$, AFIX 137 for $CH_3$), with $U_{iso}(H) = 1.2U_{eq}(CH,CH_2)$ and $U_{iso}(H) = 1.5U_{eq}(CH_3)$. Graphics were drawn with DIAMOND (version 3.2).[84]

**Computational Details.** Quantum chemical calculations were performed with the ORCA electronic structure program package.[85] All geometry optimizations were run with tight convergence criteria, using the B3LYP[86] functional together with the new efficient RIJCOSX algorithm[87] and the def2-TZVP basis set.[88] The [SD(28,MWB)] effective core potential (ECP) was used for Ru atoms.[89] In all optimizations and energy evaluations, the latest Grimme's semi-empirical atom-pairwise correction, accounting for the major part of the contribution of dispersion forces to the energy, was included.[90] From these geometries all reported data were obtained by means of single-point (SP) calculations using the same functional as well as the more polarized def2-TZVPP basis set. Bond strengths were characterized by the Wiberg bond index (WBI).[91] The topological analysis of the electronic charge density within Bader's atoms-in-molecules (AIM) methodology[92] was conducted using the AIM2000 software.[93]

**Hydrolysis Studies.** The aquation of complexes (~0.5 mM) was monitored by $^1H$ NMR spectroscopy in 25% MeOD/75% $D_2O$ (v/v) at 37 °C by using a 600 MHz Bruker Avance NMR spectrometer.

**Hydrophobicity Determinations.** Relative hydrophobicity measurements by RP-UPLC were performed using a Waters Acquity UPLC system (Waters, Milford, MA, USA), which was interfaced to quadrupole, high resolution, TOF mass spectrometer (HR-QTOF maXis impact, Bruker, Bremen, Germany), using an orthogonal Z-spray ESI interface operating in positive ion mode. The UPLC separation was performed using an Acquity UPLC BEH C18 1.7 $\mu$m particle size analytical column 50 mm × 2.1 mm (Waters) at a flow rate of 0.25 mL/min. The mobile phases used were A = $H_2O$ with 0.2% HCOOH and B = acetonitrile. The percentage of organic modifier (B) was changed linearly as follows: 0 min, 20%; 1 min, 30%; 8 min, 99%; 8.50 min, 99%; 9.50 min, 20%. Nitrogen (from a nitrogen generator) was used as the drying gas and nebulizing gas. The gas flow was set at 320 L/h

TOF-MS resolution was approximately 45.000 at full width half-maximum (fwhm) in V-mode and 17.500 fwhm in W mode, at $m/z$ 556.2771. MS data were acquired over an $m/z$ range of 50–1500. The microchannel plate (MCP) detector potential was set to 1780 V. A capillary voltage of 4.5 kV and cone voltage of 25 V were used. The interface temperature was set to 350 °C and the source temperature to 120 °C. The column temperature was set to 25 °C.

Calibrations were conducted from $m/z$ 50 to 1500 with a 1:1 mixture of 0.01 M NaOH/5% HCOOH diluted (1:5) with isopropanol/water (1:1), at a flow rate of 180 $\mu$L/h.

MS data were acquired in centroid mode and were processed by the DataAnalysis application manager (within Compass 1.7; Bruker Corporation).

Samples were dissolved in 10% v/v methanol in water, ~10 $\mu$M.

**Cell Lines and Culture Media.** Human colorectal adenocarcinoma (HT29) and EA.hy926 cell lines were acquired from the American Type Tissue Culture Collection (ATCC, USA). The 5637 (human bladder cancer cells), A427 and LCLC-103H (both human lung carcinoma cells), and SISO (human uterine cervical adenocarcinoma cells) were acquired from the German Collection of Microorganisms and Cell Cultures (DSMZ) (Braunschweig, Germany), while the ovarian carcinoma cell line A2780 and the cisplatin-resistant A2780cis were obtained from European Collection of Animal Cell Culture (ECACC, Salisbury, U.K.). These last cell lines were cultured in the RPMI-1640 medium, HT29 in the Dulbecco's modified Eagle medium (DMEM) with a high content of glucose (4.5 g/L). The EA.hy926


DOI: 10.1021/acs.jmedchem.5b01194
J. Med. Chem. 2015, 58, 7310–7327

cells were all cultured in DMEM medium but with a low glucose (1 g/L) concentration. All media were supplemented with fetal bovine serum (FBS) 10%, glutamine 1 mM, and pennicillin and streptomycin. For EA.hy926 cells DMEM medium was also supplemented with pyruvate, 2 mM.

**Cytotoxicity Assays.** A suspension of 2000 cells in 200 $\mu$L of culture medium was seeded into each well of a 96-well plate for all cell lines except for EA.hy926 cells (5000 cells for this cell line) and left at 37 °C in a 5% or 10% $CO_2$ atmosphere for 24 h. Independently, a solution of one of the metal compounds in DMF at 12.5 mM concentration was prepared. From this, successive 1:1 dilutions were performed, obtaining a total of eight solutions of concentrations ranging from 12.5 to 0.0976 mM, all of them in DMF. In turn, eight solutions were prepared by diluting 50 $\mu$L of each DMF solution in 2450 $\mu$L of the culture medium (dilution 1:50, DMF 2%). Finally, an amount of 50 $\mu$L of these last eight solutions was added to the 200 $\mu$L present in the wells. The highest final concentration of the wells was 50 $\mu$M (1/250 dilution from the original DMF solution). In all cases, the wells have a concentration of 0.4% DMF. Cells were left for 48 h in the incubator (37 °C). The crystal violet staining method was used for quantifying growth inhibition as previously described.[66] The absorbance at $\lambda$ = 570 nm was measured in a Fluostar Omega spectrophotometer.

Absorbances at each compound concentration were translated into inhibition percentages, I%, according to the following equation,

$$\mathrm{I\%} = \left[1 - \frac{A_T}{A_C}\right] \times 100 \tag{3}$$

where $A_T$ and $A_C$ are the absorbances of treated and control cells, respectively.

$IC_{50}$ values were obtained from a three-parameter fitting of the semilogarithmic curves (I% as a function of the logarithm of the concentration of compound), according to eq 4,

$$\mathrm{I\%} = \frac{I_{max}}{1 + \left(\frac{IC_{50}}{C}\right)^n} \tag{4}$$

where $I_{max}$ is the maximum inhibition observed (i.e., the inhibition observed at the highest inhibitor concentration), $IC_{50}$ is the concentration at which 50% of the cell population is live (or dead), $C$ is the compound concentration at which the inhibition I% is observed, and $n$ is the slope of the curve at the $IC_{50}$ value. The fitting was performed by using SigmaPlot 11.0 software. $IC_{50}$ values are given as errors with confidence levels higher than 95% ($p \leq 0.05$, Student's $t$ test). All compounds were tested in three independent studies with quadruplicate points. The in vitro studies were performed in the SACE service (Support Service for Experimental Sciences, University of Murcia, Murcia, Spain).

All studies except with EA.hy926 cells (DMSO for this cell line) were performed with a maximum DMF concentration of 0.4% (except for cisplatin, water diluted), and in all the experiments measurements were corrected with a water control.

**Cell Cycle Arrest Assays.** Cell cycle arrest studies were performed on SISO and 5637 cell lines. Ten-thousand cells were seeded in six-well plates and left at 37 °C in a 5% or 10% $CO_2$ atmosphere for 24 h. After that, the corresponding compound at a $IC_{50}$ concentration was added to each well (one was left without any compound, i.e., as a control). Cells were left with the compounds for an additional 24 h and then removed from the wells with trypsin, collected, and centrifuged (250$g$, 10 min). The supernatant was removed, cells washed with DMEM medium, and again centrifuged (same conditions). The supernatant was also removed, and the cells were treated with ethanol at 70% (phosphate buffered saline, PBS, 30%) for 45 min at 4 °C, and ethanol was removed by centrifugation. Cells were resuspended in PBS, and finally, RNase solution and propidium iodide (at final concentrations of 0.1 and 40 mg/mL, respectively) were added. Cells were incubated in this medium for 30−60 min. Propidium iodide (PI) fluorescence was measured for each cell in a Becton-Dickinson FACScalibur flow cytometer. In each case 30 000 events were acquired.

**Apoptosis Experiments.** For apoptosis determination assays, 1.5 × $10^5$ cells were typically seeded in a six-well plate. Ovarian cancer cells with compounds and their control were incubated, collected, and washed twice with PBS as described above (no PBS/ethanol mix was used in this case). After removal of the PBS, 40 $\mu$L of a solution containing annexin V and PI (annexin-V-Fluos from Roche) and 160 $\mu$L of incubation buffer (hepes 10 mM, NaCl 140 mM, $CaCl_2$ 5 mM, pH = 7.4) was added to the cell pellet. Cells were resuspended in this solution and left at room temperature in dark for 15 min. Then 200 $\mu$L of PBS was added immediately previous to the measurements. These were carried out in a Beckman Coulter Epics XL flow cytometer, registering the emission at wavelengths of $\lambda$ = 620 and 525 nm for PI and annexin V, respectively. In each case, 10 000 events were acquired.

**Caspase-3 Assay.** A2780 were plated in six-well sterile plates at a density of 1 × $10^6$ cells/well with 5 mL of complete medium and incubated with 2 $\mu$M compounds **3a**, **4a**, **3d**, and **4d** for 24 h after attachment to the culture surface. For caspase-3 assay, the medium was added by pipetting to a 15 mL Falcon tube. Then 1 mL of tripsin (0.25% tripsin, 0.53 mM EDTA) was added to remove cells of well surface and added to the 15 mL Falcon tube. Tubes were centrifuged at 3000 rpm at 4 °C, discarding the supernatant, and cells were collected. At this point, cells were washed with 1 mL of PBS and transferred to an Eppendorf tube. This was followed by centrifugation (10 000$g$, 1 min), discarding the supernatant. Cell lysis buffer was added, and cells were left for 10 min in ice. Then cells were centrifuged at 10 000$g$ for 1 min, and an amount of 50 $\mu$L of supernatant was added in 96-well plate with 50 $\mu$L of reaction buffer and DTT. Finally, an amount of 5 $\mu$L of DEVD-Na 200 $\mu$M was added and plate was incubated for 1 h at 37 °C in dark. Absorbance were measured at 405 nm in Fluorstar Omega spectrophotometer.

**Intracellular Reactive Oxygen Species (ROS) Determination.** Intracellular ROS were quantified to determine the oxidative stress in A2780 cells after the treatment with 2 or 1 $\mu$M for 18 h of compounds **3g** and **4g**. A2780 cells (25 × $10^3$) were seeded on 96-well plates and left attached overnight. Untreated cells containing maximal concentration of DMSO used in the treatment (0.4%) were used as a control. The treated cells were loaded with 25 $\mu$M DCFH-DA and incubated for 45 min at 37 °C before added compounds. Fluorescence was measured on FLUOstar Galaxy spectrophotometer (excitation/emission wavelengths: 485 nm/530 nm). Experiments were repeated in triplicate.

**Metal Cellular Accumulation Studies.** Ovarian cancer cells were plated in a six-well cell culture plate at a density of $10^6$ cells/well and maintained at 37 °C in a 5% $CO_2$ atmosphere. Compounds **3b**, **3c**, and **3g** were added to cells for 24 h at 2 $\mu$M concentration. Cells were harvested from the plate by using EDTA−trypsin and centrifuged at 200$g$ for 5 min. Cell pellet from each compound was washed with 1 mL of PBS. Cells were counted, transferred to Eppendorf tubes, and centrifuged at 10 000$g$ for 5 min at 4 °C. The supernatant was discarded, and pellet was digested with 100 $\mu$L of subboiled 65% $HNO_3$ (subboiled suprapur 65% nitric acid, Merck) overnight. Afterward, intracellular ruthenium concentrations were measured by flameless atomic absorption spectrometry. An atomic absorption spectrometer (model 800, Perkin-Elmer, Shelton, USA) equipped for Zeeman-effect background correction, with a transversely heated graphite tube atomizer and AS-800 autosampler, was used. The autosampler was not used, and the samples were pipetted manually into the atomizer. Pyrolytic graphite platforms in pyrolytically coated tubes were obtained from the same manufacturer (part number B050-4033). Argon at 250 mL $min^{-1}$ was used as inert gas except during atomization, when it was stopped. Ruthenium hollow cathode lamp (Perkin-Elmer) was used as the radiation sources. Probes were injected at a volume of 20 $\mu$L into regular graphite wall tubes. All the measurements were done in triplicate.

**DNA Binding in Cells.** A2780 cells grown in a Petri cell culture dish were exposed to 2 $\mu$M **3g** or **4g** for 24 h. After incubation period cells were trypsinized and washed twice in ice-cold PBS. Cells were then lysed in DNAzol (DNAzols genomic DNA isolation reagent,


DOI: 10.1021/acs.jmedchem.5b01194
J. Med. Chem. 2015, 58, 7310−7327

MRC) supplemented with RNase A (100 mg $mL^{-1}$). The genomic DNA was precipitated from the lysate with 75% ethanol−water, dried, and resuspended in water. The DNA content in each sample was determined by spectrophotometer NanoDrop ND-1000. Concentrations of iridium and ruthenium were measured by AAS. Experiments were performed in triplicate, and the values are the mean ± SD.

**Endothelial Tube Formation Assay.** Unpolymerized Matrigel (8.7 mg/mL; B&D Biosciences, Bedford, MA) was placed in 96-well plates (9 μL/well) and allowed to polymerize for 1 h at 37 °C. This study revealed that tube formation was maximal after 16 h at the concentration of 12 × $10^3$ cells/well for EA.hy926. EA.hy926 cells were suspended in medium without FBS at different concentrations of each compound. The cells were seeded on top of the Matrigel layer and incubated at 37 °C. After 16 h for EA.hy926 cells, the wells were photographed by using an inverted phase-contrast microscope (Nikon mod. Eclipse TE-2000-U). EA.hy926 cells formed capillary-like networks with different tube morphology. Tube formation was quantified by measuring the total length of the tube network, number of network, and area of network under 4× magnification using ImageJ software (National Institutes of Health, Bethesda, MD, USA).

**Statistical Analysis.** To compare independent groups of numerical data, Student's *t*-test was used. All statistical analyses were performed using SigmaPlot 11.

**Ethidium Bromide and Hoechst 33258 Displacement Experiments.** An amount of 3 mL of a solution, that is, 10 μM DNA and 0.33 μM EB (saturated binding levels[94]), in Tris buffer was titrated with aliquots of a concentrated solution of the complex producing solutions with varied mole ratios of complex to ct-DNA. After each addition the solution was stirred for 5 min before measurement. The fluorescence spectra of the solution were obtained by exciting at $\lambda$ = 520 nm and measuring the emission spectra from $\lambda$ = 530−700 nm with 5 nm slits. The procedure was the same for the Hoechst 33258 reactions using the following conditions: working solutions were 20 μM DNA and 2 μM Hoechst 33258; $\lambda_{ex}$ = 338 nm, and the emission spectra were measured at $\lambda$ = 350−650 nm (with $\lambda_{max}$ = 462 nm).

**Reaction with Human Serum Albumin (HSA). Procedures for Fluorescence Quenching Studies.** The stock solutions of proteins (6.5 × $10^{-6}$ mol $L^{-1}$) were prepared by dissolving the solid HSA in 50 mM Tris-HCl, 100 mM NaCl buffer of pH 7.4 and storing at 0−4 °C in the dark for about a week. The concentrations of HSA were determined from optical density measurements, by using $\varepsilon_{278}$ = 36 000 $M^{-1}$ $cm^{-1}$.[79]

Quantitative analyses of the interaction between complex **3d** and HSA were performed by fluorimetric titration. A 3.0 mL portion of aqueous solution of protein (5 × $10^{-6}$ mol $L^{-1}$) was titrated by successive additions of complex solution (to give a final concentration of 32.5 × $10^{-6}$ mol $L^{-1}$). Titrations were done manually by using a trace syringe. For every addition, the mixture solution was shaken and allowed to stand for 15 min and then the fluorescence intensities were measured with an excitation wavelength of $\lambda$ = 295 nm and emission wavelengths in the interval $\lambda$ = 300−550 nm. The width of the excitation and emission slit was set to 5 nm. To decrease the inner filtering effects due to high optical densities of probe, front-face illumination is performed.[95] In the meantime, the synchronous fluorescence intensity of the mixture solution was measured at $\Delta\lambda$ = 15 nm and $\Delta\lambda$ = 60 nm, respectively.

**Site Marker Competitive Experiments.** Binding location studies between complex **3d** and HSA in the presence of two site markers (warfarin and ibuprofen) were measured using the fluorescence titration methods.[79]

*Warfarin as Marker of Site I.* The displacement experiments were performed using the site probe warfarin by preparing equimolar mixtures of protein and warfarin (each 1 × $10^{-6}$ mol $L^{-1}$), which were then thoroughly mixed and equilibrated at room temperature for 1 h. A 3.0 mL portion of the solution was transferred to the spectrofluorimetric cell, and then it was titrated by successive additions of complex **3d** solution. After thorough mixing of the resultant solution at each titration step, the solutions were allowed to stand for 20 min. An excitation wavelength of 320 nm was selected. The width of the excitation and emission slit was set to $\lambda$ = 5 nm, and the emission fluorescence spectra were recorded in the wavelength range $\lambda$ = 340−600 nm.

*Ibuprofen as Marker of Site II.* Equimolar mixtures of protein and complex **3d** (1 × $10^{-6}$ mol $L^{-1}$) were thoroughly mixed and allowed to equilibrate at room temperature for 1 h. A 3.0 mL portion of the solution was transferred to the spectrofluorimetric cell, and then ibuprofen was gradually added to this solution. The procedure was the same as that in the displacement experiments using the site probe warfarin.

## ■ ASSOCIATED CONTENT

### Supporting Information

The Supporting Information is available free of charge on the ACS Publications website at DOI: 10.1021/acs.jmedchem.5b01194.

Additional crystallographic data, figures for cell cycle analysis, apoptosis, Hoechst 33258 displacement experiment; **3d** and **4d** NMR spectra (PDF)
Crystallographic file for **4d** (CIF)
Crystallographic file for **3d** (CIF)
Molecular formula strings (CSV)

Single crystal X-ray data have been deposited as CCDC deposition numbers 1061745 (**3d**) and 1061746 (**4d**) with the Cambridge Crystallographic Data Centre, from which it can be obtained upon request at www.ccdc.cam.ac.uk/data_request/cif.

## ■ AUTHOR INFORMATION

### Corresponding Author

*E-mail: jruiz@um.es. Fax: +34 868 884148. Phone: +34 868 887455.

### Notes

The authors declare no competing financial interest.

## ■ ACKNOWLEDGMENTS

This work was supported by the Spanish Ministerio de Economía y Competitividad and FEDER (Project SAF2011-26611) and by Fundación Séneca-CARM (Projects 08666/PI/08 and 15354/PI/10). G.Y. thanks the European Union Seventh Framework Programme—Marie Curie Co-fund (FP7/2007−2013) under U-IMPACT Grant Agreement 267143. COST Action CM1105 is also gratefully acknowledged for providing opportunities for discussion and a Short Term Scientific Mission (STSM) to A.D. Professor Ignacio López is also acknowledged for AAS assistance.

## ■ REFERENCES

(1) Rosenberg, B.; VanCamp, L.; Trosko, J. E.; Mansour, V. H. Platinum compounds: a new class of potent antitumour agents. *Nature* **1969**, *222*, 385−386.
(2) Kelland, L. The resurgence of platinum-based cancer chemotherapy. *Nat. Rev. Cancer* **2007**, *7*, 573−584.
(3) Medici, S.; Peana, M.; Nurchi, V. M.; Lachowicz, J. I.; Crisponi, G.; Zoroddu, M. A. Noble metals in medicine: latest advances. *Coord. Chem. Rev.* **2015**, *284*, 329−350.
(4) Bergamo, A.; Gaiddon, C.; Schellens, J. H.; Beijnen, J. H.; Sava, G. Approaching tumour therapy beyond platinum drugs: status of the art and perspectives of ruthenium drug candidates. *J. Inorg. Biochem.* **2012**, *106*, 90−99.
(5) Rademaker-Lakhai, J. M.; van den Bongard, D.; Pluim, D.; Beijnen, J. H.; Schellens, J. H. A phase I and pharmacological study with imidazolium-trans-DMSO-imidazole-tetrachlororuthenate, a


DOI: 10.1021/acs.jmedchem.5b01194
J. Med. Chem. 2015, 58, 7310−7327

novel ruthenium anticancer agent. *Clin. Cancer Res.* **2004**, *10*, 3717−3727.
(6) Suntharalingam, K.; Lin, W.; Johnstone, T. C.; Bruno, P. M.; Zheng, Y. R.; Hemann, M. T.; Lippard, S. J. A breast cancer stem cell-selective, mammospheres-potent osmium(VI) nitrido complex. *J. Am. Chem. Soc.* **2014**, *136*, 14413−14416.
(7) Stimpson, S.; Jenkinson, D. R.; Sadler, A.; Latham, M.; Wragg, D. A.; Meijer, A. J.; Thomas, J. A. Tuning the excited state of water-soluble Ir(III)-based DNA intercalators that are isostructural with $[Ru(II)(NN)_2(dppz)]$ light-switch complexes. *Angew. Chem., Int. Ed.* **2015**, *54*, 3000−3003.
(8) Gill, M. R.; Thomas, J. A. Ruthenium(II) polypyridyl complexes and DNA-from structural probes to cellular imaging and therapeutics. *Chem. Soc. Rev.* **2012**, *41*, 3179−3192.
(9) Leung, C.-H.; Zhong, H.-J.; Yang, H.; Cheng, Z.; Chan, D. S.-H.; Ma, V. P.; Abagyan, R.; Wong, C.-Y.; Ma, D.-L. A metal-based inhibitor of tumor necrosis factor-$\alpha$. *Angew. Chem., Int. Ed.* **2012**, *51*, 9010−9014.
(10) Man, B. Y.-W; Chan, H.-M.; Leung, C.-H.; Chan, D. S.-H.; Bai, L.-P.; Jiang, Z.-H.; Li, H.-W.; Ma, D.-L. Group 9 metal-based inhibitors of $\beta$-amyloid (1−40) fibrillation as potential therapeutic agents for Alzheimer's disease. *Chem. Sci.* **2011**, *2*, 917−921.
(11) Leung, C.-H.; Zhong, H.-J.; Chan, D. S.-H.; Ma, D.-L. Bioactive iridium and rhodium complexes as therapeutic agents. *Coord. Chem. Rev.* **2013**, *257*, 1764−1776.
(12) Leung, C.-H.; He, H.-Z.; Liu, L.-J.; Wang, M.; Chan, D. S.-H.; Ma, D.-L. Metal complexes as inhibitors of transcription factor activity. *Coord. Chem. Rev.* **2013**, *257*, 3139−3151.
(13) Barry, N. P. E.; Sadler, P. J. Exploration of the medical periodic table: towards new targets. *Chem. Commun.* **2013**, *49*, 5106−5131.
(14) Scolaro, C.; Bergamo, A.; Brescacin, L.; Delfino, R.; Cocchietto, M.; Laurenczy, G.; Geldbach, T. J.; Sava, G.; Dyson, P. J. *In vitro* and *in vivo* evaluation of ruthenium(II)−arene PTA complexes. *J. Med. Chem.* **2005**, *48*, 4161−4171.
(15) Gasser, G.; Ott, I.; Metzler-Nolte, N. Organometallic Anticancer Compounds. *J. Med. Chem.* **2011**, *54*, 3−25.
(16) Leonidova, A.; Gasser, G. Underestimated potential of organometallic rhenium complexes as anticancer agents. *ACS Chem. Biol.* **2014**, *9*, 2180−2193.
(17) Hartinger, C. G.; Dyson, P. J. Bioorganometallic chemistry—from teaching paradigms to medicinal applications. *Chem. Soc. Rev.* **2009**, *38*, 391−401.
(18) Liu, W.; Gust, R. Metal N-heterocyclic carbene complexes as potential antitumor metallodrugs. *Chem. Soc. Rev.* **2013**, *42*, 755−773.
(19) Oehninger, L.; Rubbiani, R.; Ott, I. N-heterocyclic carbene metal complexes in medicinal chemistry. *Dalton Trans.* **2013**, *42*, 3269−3284.
(20) Metzler-Nolte, N. Biomedical applications of organometal-peptide conjugates. *Top. Organomet. Chem.* **2010**, *32*, 195−217.
(21) Cutillas, N.; Yellol, G. S.; de Haro, C.; Vicente, C.; Rodríguez, V.; Ruiz, J. Anticancer cyclometalated complexes of platinum group metals and gold. *Coord. Chem. Rev.* **2013**, *257*, 2784−2797.
(22) Süss-Fink, G. Arene ruthenium complexes as anticancer agents. *Dalton Trans.* **2010**, *39*, 1673−1688.
(23) Omae, I. Applications of five-membered ring products of cyclometalation reactions as anticancer agents. *Coord. Chem. Rev.* **2014**, *280*, 84−95.
(24) Fu, Y.; Romero, M. J.; Habtemariam, A.; Snowden, M. E.; Song, L.; Clarkson, G. J.; Qamar, B.; Pizarro, A. M.; Unwin, P. R.; Sadler, P. J. The contrasting chemical reactivity of potent isoelectronic iminopyridine and azopyridine osmium(II) arene anticancer complexes. *Chem. Sci.* **2012**, *3*, 2485−2493.
(25) Huang, H.; Zhang, P.; Yu, B.; Chen, Y.; Wang, J.; Ji, L.; Chao, H. Targeting Nucleus DNA with a Cyclometalated Dipyridophenazineruthenium(II) Complex. *J. Med. Chem.* **2014**, *57*, 8971−8983.
(26) Ma, D.-L.; Chan, D. S.-H.; Leung, C.-H. Group 9 organometallic compounds for therapeutic and bioanalytical applications. *Acc. Chem. Res.* **2014**, *47*, 3614−3631.
(27) Hartinger, C. G.; Metzler-Nolte, N.; Dyson, P. J. Challenges and Opportunities in the Development of Organometallic Anticancer Drugs. *Organometallics* **2012**, *31*, 5677−5685.
(28) Patra, M.; Gasser, G. Organometallic compounds: an opportunity for chemical biology? *ChemBioChem* **2012**, *13*, 1232−1252.
(29) Chow, M. J.; Licona, C.; Yuan Qiang Wong, D.; Pastorin, G.; Gaiddon, C.; Ang, W. H. Discovery and investigation of anticancer ruthenium−arene schiff-base complexes via water-promoted combinatorial three-component assembly. *J. Med. Chem.* **2014**, *57*, 6043−6059.
(30) Liu, Z.; Romero-Canelón, I.; Qamar, B.; Hearn, J. M.; Habtemariam, A.; Barry, N. P.; Pizarro, A. M.; Clarkson, G. J.; Sadler, P. J. The Potent Oxidant Anticancer Activity of Organoiridium Catalysts. *Angew. Chem., Int. Ed.* **2014**, *53*, 3941−3946.
(31) Clavel, C. M.; Păunescu, E.; Nowak-Sliwinska, P.; Griffioen, A. W.; Scopelliti, R.; Dyson, P. J. Discovery of a highly tumor-selective organometallic ruthenium(II)−arene complex. *J. Med. Chem.* **2014**, *57*, 3546−3558.
(32) Ruiz, J.; Vicente, C.; de Haro, C.; Bautista, D. Novel bis-C,N-cyclometalated iridium(III) thiosemicarbazide antitumor complexes: interactions with human serum albumin and DNA, and inhibition of cathepsin B. *Inorg. Chem.* **2013**, *52*, 974−982.
(33) Ruiz, J.; Rodríguez, V.; Cutillas, N.; Espinosa, A.; Hannon, M. J. A potent ruthenium(II) antitumor complex bearing a lipophilic levonorgestrel group. *Inorg. Chem.* **2011**, *50*, 9164−9171.
(34) Kandioller, W.; Hartinger, C. G.; Nazarov, A. A.; Bartel, C.; Skocic, M.; Jakupec, M. A.; Arion, V. B.; Keppler, B. K. Maltol-derived ruthenium-cymene complexes with tumor inhibiting properties: the impact of ligand-metal bond stability on anticancer activity *in vitro*. *Chem. - Eur. J.* **2009**, *15*, 12283−12291.
(35) Meier, S. M.; Hanif, M.; Adhireksan, Z.; Pichler, V.; Novak, M.; Jirkovsky, E.; Jakupec, M. A.; Arion, V. B.; Davey, C. A.; Keppler, B. K.; Hartinger, C. G. Novel metal(II) arene 2-pyridinecarbothioamides: a rationale to orally active organometallic anticancer agents. *Chem. Sci.* **2013**, *4*, 1837−1846.
(36) Folkman, J. Endogenous angiogenesis inhibitors. *APMIS* **2004**, *112*, 496−507.
(37) Aranda, E.; Owen, G. I. A semi-quantitative assay to screen for angiogenic compounds and compounds with angiogenic potential using the EA.hy926 endothelial cell line. *Biol. Res.* **2009**, *42*, 377−389.
(38) Ma, J.; Waxman, D. J. Combination of antiangiogenesis with chemotherapy for more effective cancer treatment. *Mol. Cancer Ther.* **2008**, *7*, 3670−3684.
(39) Teoh, D. G.; Secord, A. A. Antiangiogenic therapies in epithelial ovarian cancer. *Cancer Control* **2011**, *18*, 31−43.
(40) Rademaker-Lakhai, J. M.; van den Bongard, D.; Pluim, D.; Beijnen, J. H.; Schellens, J. H. A phase I and pharmacological study with imidazolium-trans-DMSO-imidazole-tetrachlororuthenate, a novel ruthenium anticancer agent. *Clin. Cancer Res.* **2004**, *10*, 3717−3727.
(41) Yang, L.; Zhang, J.; Wang, C.; Qin, X.; Yu, Q.; Zhou, Y.; Liu, J. Interaction between 8-hydroxyquinoline ruthenium(II) complexes and basic fibroblast growth factors (bFGF): inhibiting angiogenesis and tumor growth through ERK and AKT signaling pathways. *Metallomics* **2014**, *6*, 518−531.
(42) Nowak-Sliwinska, P.; van Beijnum, J. R.; Casini, A.; Nazarov, A. A.; Wagniéres, G.; van den Bergh, H.; Dyson, P. J.; Griffioen, A. W. Organometallic ruthenium(II) arene compounds with antiangiogenic activity. *J. Med. Chem.* **2011**, *54*, 3895−3902.
(43) Clavel, C. M.; Păunescu, E.; Nowak-Sliwinska, P.; Griffioen, A. W.; Scopelliti, R.; Dyson, P. J. Modulating the Anticancer Activity of Ruthenium(II)-Arene Complexes. *J. Med. Chem.* **2015**, *58*, 3356−3365.
(44) Wilbuer, A.; Vlecken, D. H.; Schmitz, D. J.; Kräling, K.; Harms, K.; Bagowski, C. P.; Meggers, E. Iridium complex with antiangiogenic properties. *Angew. Chem., Int. Ed.* **2010**, *49*, 3839−3842.
(45) Zamora, A.; Pérez, S. A.; Rodríguez, V.; Janiak, C.; Yellol, G. S.; Ruiz, J. Dual antitumor and antiangiogenic activity of organoplatinum-(II) complexes. *J. Med. Chem.* **2015**, *58*, 1320−1336.


DOI: 10.1021/acs.jmedchem.5b01194
*J. Med. Chem.* 2015, 58, 7310−7327

(46) Yellol, G. S.; Donaire, A.; Yellol, J. G.; Vasylyeva, V.; Janiak, C.; Ruiz, J. On the antitumor properties of novel cyclometalated benzimidazole Ru(II), Ir(III) and Rh(III) complexes. *Chem. Commun.* **2013**, *49*, 11533−11535.
(47) Wang, F.; Habtemariam, A.; van der Geer, E. P. L.; Fernández, R.; Melchart, M.; Deeth, R. J.; Aird, R.; Guichard, S.; Fabbiani, F. P. A.; Lozano-Casal, P.; Oswald, I. D. H.; Jodrell, D. I.; Parsons, S.; Sadler, P. J. Controlling ligand substitution reactions of organometallic complexes: tuning cancer cell cytotoxicity. *Proc. Natl. Acad. Sci. U. S. A.* **2005**, *102*, 18269−18274.
(48) Boiani, M.; González, M. Imidazole and benzimidazole derivatives as chemotherapeutic agents. *Mini-Rev. Med. Chem.* **2005**, *5*, 409−424.
(49) Bansal, Y.; Silakari, O. The therapeutic journey of benzimidazoles: a review. *Bioorg. Med. Chem.* **2012**, *20*, 6208−6236.
(50) Støving Dam, C.; Pérez Henarejos, S. A.; Tsolakou, T.; Segato, C. A.; Gammelgaard, B.; Yellol, G. S.; Ruiz, J.; Lambert, I. H.; Stürup, S. In vitro characterization of a novel C,N-cyclometalated benzimidazole Ru(II) arene complex: stability, intracellular distribution and binding, effect on organic osmolyte homeostasis and induction of apoptosis. *Metallomics* **2015**, *7*, 885−895.
(51) Martínez-Alonso, M.; Busto, N.; Jalón, F. A.; Manzano, B. R.; Leal, J. M.; Rodríguez, A. M.; García, B.; Espino, G. Derivation of structure-activity relationships from the anticancer properties of ruthenium(II) arene complexes with 2-aryldiazole ligands. *Inorg. Chem.* **2014**, *53*, 11274−11288.
(52) Lai, H.; Zhao, Z.; Li, L.; Zheng, W.; Chen, T. Antiangiogenic ruthenium(II) benzimidazole complexes, structure-based activation of distinct signaling pathways. *Metallomics* **2015**, *7*, 439−447.
(53) Yellol, G. S.; Yellol, J. G.; Kenche, V. B.; Liu, X. M.; Barnham, K. J.; Donaire, A.; Janiak, C.; Ruiz, J. Synthesis of 2-pyridyl-benzimidazole iridium(III), ruthenium(II), and platinum(II) complexes. study of the activity as inhibitors of amyloid-$\beta$ aggregation and neurotoxicity evaluation. *Inorg. Chem.* **2015**, *54*, 470−475.
(54) Bhaumik, C.; Saha, D.; Das, S.; Baitalik, S. Synthesis, structural characterization, photophysical, electrochemical, and anion-sensing studies of luminescent homo- and heteroleptic ruthenium(II) and osmium(II) complexes based on terpyridyl-imidazole ligand. *Inorg. Chem.* **2011**, *50*, 12586−12600.
(55) Maity, D.; Das, S.; Mardanya, S.; Baitalik, S. Synthesis, structural characterization, and photophysical, spectroelectrochemical, and anion-sensing studies of heteroleptic ruthenium(II) complexes derived from 4′-polyaromatic-substituted terpyridine derivatives and 2,6-bis(benzimidazol-2-yl)pyridine. *Inorg. Chem.* **2013**, *52*, 6820−6838.
(56) Seršen, S.; Kljun, J.; Kryeziu, K.; Panchuk, R.; Alte, B.; Körner, W.; Heffeter, P.; Berger, W.; Turel, I. Structure-Related Mode-of-Action Differences of Anticancer Organoruthenium Complexes with $\beta$-Diketonates. *J. Med. Chem.* **2015**, *58*, 3984−3996.
(57) Barnes-Seeman, D.; Beck, J.; Springer, C. Fluorinated compounds in medicinal chemistry: recent applications, synthetic advances and matched-pair analyses. *Curr. Top. Med. Chem.* **2014**, *14*, 855−864.
(58) Cutillas, N.; Martínez, A.; Yellol, G. S.; Rodríguez, V.; Zamora, A.; Pedreño, M.; Donaire, A.; Janiak, C.; Ruiz, J. Anticancer C,Ncycloplatinated(II) complexes containing fluorinated phosphine ligands: synthesis, structural characterization, and biological activity. *Inorg. Chem.* **2013**, *52*, 13529−13535.
(59) Boutadla, Y.; Davies, D. L.; Jones, R. C.; Singh, K. The scope of ambiphilic acetate-assisted cyclometallation with half-sandwich complexes of iridium, rhodium and ruthenium. *Chem. - Eur. J.* **2011**, *17*, 3438−3448.
(60) (a) Ruiz, J.; Rodríguez, V.; de Haro, C.; Espinosa, A.; Pérez, J.; Janiak, C. New 7-azaindole palladium and platinum complexes: crystal structures and theoretical calculations. In vitro anticancer activity of the platinum compounds. *Dalton Trans.* **2010**, *39*, 3290−3301. (b) Ruiz, J.; Villa, M. D.; Rodríguez, V.; Cutillas, N.; Vicente, C.; López, G.; Bautista, D. A novel metal-binding mode of thymine nucleobases: N3 and O4 chelation. *Inorg. Chem.* **2007**, *46*, 5448−5449. (c) Althoff, G.; Ruiz, J.; Rodríguez, V.; López, G.; Pérez, J.; Janiak, C. Can a single **C**−H···F−**C** hydrogen bond make a difference? Assessing the H···F bond strength from 2-D $^{1}$H-$^{19}$F CP/MAS NMR. *CrystEngComm* **2006**, *8*, 662−665.
(61) (a) Habib, H. A.; Hoffmann, A.; Höppe, H. A.; Steinfeld, G.; Janiak, C. Crystal structure solid-state cross polarization magic angle spinning $^{13}$C NMR correlation in luminescent $d^{10}$ metal-organic frameworks constructed with the 1,2-Bis(1,2,4-triazol-4-yl)ethane ligand. *Inorg. Chem.* **2009**, *48*, 2166−2180. (b) Wisser, B.; Janiak, C. Chiral metal complexes with the biologically active (+)-pilocarpine ligand: $[MCl_2(\kappa N\text{-}(+)\text{-pilocarpine})_2]$ (M = Co, Cu). *Z. Anorg. Allg. Chem.* **2007**, *633*, 1796−1800.
(62) Desiraju, G. R.; Steiner, T. The Weak Hydrogen Bond. In *IUCr Monograph on Crystallography*; Oxford Science: Oxford, U.K., 1999; Vol. *9*.
(63) (a) Nishio, M. The CH/$\pi$ hydrogen bond in chemistry. Conformation, supramolecules, optical resolution and interactions involving carbohydrates. *Phys. Chem. Chem. Phys.* **2011**, *13*, 13873−13900. (b) Nishio, M.; Umezawa, Y.; Honda, K.; Tsuboyama, S.; Suezawa, H. CH/$\pi$ hydrogen bonds in organic and organometallic chemistry. *CrystEngComm* **2009**, *11*, 1757−1788. (c) Nishio, M. CH/$\pi$ hydrogen bonds in crystals. *CrystEngComm* **2004**, *6*, 130−158. (d) Janiak, C.; Temizdemir, S.; Dechert, S.; Deck, W.; Girgsdies, F.; Heinze, J.; Kolm; Mario, J.; Scharmann; Tobias, G.; Zipffel, O. M. Binary [Hydrotris(indazol-1-yl)borato]metal Complexes, $M(Tp_4^{Bo})_2$[1] with M = Fe, Co, Ni, Cu, and Zn: Electronic Properties and Solvent-Dependent Framework Structures through C−H···$\pi$ Interactions. *Eur. J. Inorg. Chem.* **2000**, *2000*, 1229−1241. (e) Umezawa, Y.; Tsuboyama, S.; Honda, K.; Uzawa, J.; Nishio, M. CH/$\pi$ Interaction in the Crystal Structure of Organic Compounds. A Database Study. *Bull. Chem. Soc. Jpn.* **1998**, *71*, 1207−213. (f) Nishio, M. H.; Hirota, M.; Umezawa,Y. *The CH/π Interaction (Evidence, Nature and Consequences)*; Wiley-VCH: New York, 1998.
(64) (a) Yang, X.-J.; Drepper, F.; Wu, B.; Sun, W.-H.; Haehnel, W.; Janiak, C. From model compounds to protein binding: syntheses, characterizations and fluorescence studies of $[Ru^{II}(bipy)(terpy)L]^{2+}$ complexes (bipy = 2,2′-bipyridine; terpy = 2,2′:6′,2″-terpyridine; L = imidazole, pyrazole and derivatives, cytochrome c. *Dalton Trans.* **2005**, 256−267. (b) Janiak, C. A critical account on $\pi$−$\pi$ stacking in metal complexes with aromatic nitrogen-containing ligands. *J. Chem. Soc., Dalton Trans.* **2000**, 3885−3896.
(65) Millett, A. J.; Habtemariam, A.; Romero-Canelón, I.; Clarkson, G. J.; Sadler, P. J. Contrasting Anticancer Activity of Half-Sandwich Iridium(III) Complexes Bearing Functionally Diverse 2-Phenylpyridine Ligands. *Organometallics* **2015**, *34*, 2683−2694.
(66) Bracht, K.; Boubakari; Grünert, R.; Bednarski, P. J. Correlations between the activities of 19 antitumor agents and the intracellular glutatione concentrations in a panel of 14 human cancer cell lines: comparisons with the National Cancer Institute data. *Anti-Cancer Drugs* **2006**, *11*, 41−51.
(67) Wang, D.; Lippard, S. J. Cellular processing of platinum anticancer drugs. *Nat. Rev. Drug Discovery* **2005**, *4*, 307−320.
(68) Kelland, L. R.; Barnard, C. F.; Mellish, K. J.; Jones, M.; Goddard, P. M.; Valenti, M.; Bryant, A.; Murrer, B. A.; Harrap, K. R. A novel trans-platinum coordination complex possessing in vitro and in vivo antitumor activity. *Cancer Res.* **1994**, *54*, 5618−5622.
(69) Novohradsky, V.; Zerzankova, L.; Stepankova, J.; Kisova, A.; Kostrhunova, H.; Liu, Z.; Sadler, P. J.; Kasparkova, J.; Brabec, V. A dual-targeting, apoptosis-inducing organometallic half-sandwich iridium anticancer complex. *Metallomics* **2014**, *6*, 1491−1501.
(70) Salvesen, G. S.; Riedl, S. J. Caspase mechanisms. *Adv. Exp. Med. Biol.* **2008**, *615*, 13−23.
(71) Gurtu, V.; Kain, S. R.; Zhang, G. Fluorometric and colorimetric detection of caspase activity associated with apoptosis. *Anal. Biochem.* **1997**, *251*, 98−102.
(72) Robinson, J. P.; Bruner, L. H.; Bassoe, C. F.; Hudson, J. L.; Ward, P. A.; Phan, S. H. Measurement of intracellular fluorescence of human-monocytes relative to oxidativemetabolism. *J. Leukocyte Biol.* **1988**, *43*, 304−310.


DOI: 10.1021/acs.jmedchem.5b01194
*J. Med. Chem.* 2015, 58, 7310−7327

(73) Kalyanaraman, B.; Darley-Usmar, V.; Davies, K. J.; Dennery, P. A.; Forman, H. J.; Grisham, M. B.; Mann, G. E.; Moore, K.; Roberts, L. J.; Ischiropoulos, H. Measuring reactive oxygen and nitrogen species with fluorescent probes: challenges and limitations. *Free Radical Biol. Med.* **2012**, *52*, 1−6.
(74) Kragh-Hansen, U. Molecular aspects of ligand binding to serum albumin. *Pharmacol. Rev.* **1981**, *33*, 17−53.
(75) Brown, J. R. In *Albumin Structure, Function, and Uses*; Rosenoer, V. M., Oratz, M., Rothschild, M. A., Eds.; Pergamon Press: Oxford, U.K., 1977; pp 27−51.
(76) Timerbaev, A. R.; Hartinger, C. G.; Aleksenko, S. S.; Keppler, B. K. Interactions of antitumor metallodrugs with serum proteins: advances in characterization using modern analytical methodology. *Chem. Rev.* **2006**, *106*, 2224−2248.
(77) Lease, N.; Vasilevski, V.; Carreira, M.; de Almeida, A.; Sanaú, M.; Hirva, P.; Casini, A.; Contel, M. Potential Anticancer Heterometallic Fe−Au and Fe−Pd Agents: Initial Mechanistic Insights. *J. Med. Chem.* **2013**, *56*, 5806−5818.
(78) Lakowicz, J. R. *Principles of Fluorescence Spectroscopy*, 3rd ed.; Springer: New York, 2006.
(79) Samari, F.; Hemmateenejad, B.; Shamsipur, M.; Rashidi, M.; Samouei, H. Affinity of Two Novel Five-Coordinated Anticancer Pt(II) Complexes to Human and Bovine Serum Albumins: A Spectroscopic Approach. *Inorg. Chem.* **2012**, *51*, 3454−3464.
(80) Guan, Y.; Shi, R.; Li, X.; Zhao, M.; Li, Y. Multiple binding modes for dicationic hoechst 33258 to DNA. *J. Phys. Chem. B* **2007**, *111*, 7336−7344.
(81) Khoo, C. P.; Micklem, K.; Watt, S. M. A comparison of methods for quantifying angiogenesis in the Matrigel assay in vitro. *Tissue Eng., Part C* **2011**, *17*, 895−906.
(82) Sheldrick, G. M. A short history of SHELX. *Acta Crystallogr., Sect. A: Found. Crystallogr.* **2008**, *64*, 112−122.
(83) Sheldrick, G. M. *Program SADABS*; University of Göttingen: Göttingen, Germany, 1996.
(84) *DIAMOND 3.2 for Windows*; Crystal Impact Gbr: Bonn, Germany; http://www.crystalimpact.com/diamond.
(85) Neese, F. *ORCA—An ab Initio, DFT and Semiempirical SCF-MO Package*, version 3.0.2; Max Planck Institute for Bioinorganic Chemistry: Mülheim an der Ruhr, Germany, 2012; https://orcaforum.cec.mpg.de/. Neese, F. The ORCA program system. *WIREs Comput. Mol. Sci.* **2012**, *2*, 73−78.
(86) (a) Becke, A. D. Semiempirical hybrid functional with improved performance in an extensive chemical assessment. *J. Chem. Phys.* **1993**, *98*, 5648−5652. (b) Lee, C. T.; Yang, W. T.; Parr, R. G. Development of the Colle-Salvetti correlation-energy formula into a functional of the electron density. *Phys. Rev. B: Condens. Matter Mater. Phys.* **1988**, *37*, 785−789.
(87) Neese, F.; Wennmohs, F.; Hansen, A.; Becker, U. Efficient, approximate and parallel Hartree−Fock and hybrid DFT calculations. A 'chain-of-spheres' algorithm for the Hartree−Fock exchange. *Chem. Phys.* **2009**, *356*, 98−109.
(88) (a) Schäfer, A.; Huber, C.; Ahlrichs, R. *J. Chem. Phys.* **1994**, *100*, 5829−5835. (b) Weigend, F.; Ahlrichs, R. Balanced basis sets of split valence, triple zeta valence and quadruple zeta valence quality for H to Rn: Design and assessment of accuracy. *Phys. Chem. Chem. Phys.* **2005**, *7*, 3297−3305.
(89) Andrae, D.; Häussermann, U.; Dolg, M.; Stoll, H.; Preuss, H. Energy-adjusted ab initio pseudopotentials for the second and third row transition elements. *Theor. Chim. Acta* **1990**, *77*, 123−141 ECP parameters for Ru [SD(28,MWB)] have been obtained from the pseudopotential library of the Stuttgart/Cologne group at http://www.uni-stuttgart.de/theochem/.
(90) Grimme, S.; Antony, J.; Ehrlich, S.; Krieg, H. *J. Chem. Phys.* **2010**, *132*, 154104.
(91) Wiberg, K. *Tetrahedron* **1968**, *24*, 1083−1096.
(92) (a) Bader, R. F. W. In *Atoms in Molecules: A Quantum Theory*; Oxford University Press: Oxford, U.K., 1990. (b) Bader, R. F. W. *Chem. Rev.* **1991**, *91*, 893−928. (c) Matta, C. F.; Boyd, R. J. In *The Quantum Theory of Atoms in Molecules*; Matta, C. F., Boyd, R. J., Eds.; Wiley-VCH: New York, 2007; pp 1−34.
(93) (a) Biegler-König, F.; Schönbohm, J. *AIM2000*, version 2.0; Büro für Innovative Software: Bielefeld, Germany, 2002; http://www.aim2000.de/. Biegler-König, F.; Schönbohm, J.; Bayles, D. *J. Comput. Chem.* **2001**, *22*, 545−559. (b) Biegler-König, F.; Schönbohm, J. Update of the AIM2000-program for atoms in molecules. *J. Comput. Chem.* **2002**, *23*, 1489−1494.
(94) Barton, J. K.; Goldberg, J. M.; Kumar, C. V.; Turro, N. J. Binding modes and base specificity of tris(phenanthroline)ruthenium-(II) enantiomers with nucleic acids: tuning the stereoselectivity. *J. Am. Chem. Soc.* **1986**, *108*, 2081−2088.
(95) Valeur, B.; Berberan-Santos, M. N. *Molecular Fluorescence: Principles and Applications*, 2nd ed.; Wiley-VCH: Weinheim, Germany, 2012.


DOI: 10.1021/acs.jmedchem.5b01194
*J. Med. Chem.* 2015, 58, 7310−7327